Università degli Studi di Catania

Dipartimento di Ingegneria Elettrica, Elettronica e Informatica

---

International Ph.D. course in Systems Engineering - XXVII cycle

Ph.D. Thesis

Nonlinear oscillations in high power systems

Marco Iachello

Tutor: Prof. M. Frasca
Coordinator: Prof. L. Fortuna

Contents

Preface

The main topic of this work is to investigate on nonlinear phenomena affecting high power systems and on the strategies adopted to model them. In the first chapter the attention is focused on two big areas of high power systems: power electronics and systems/devices used to sustain plasma fusion. Although it is common that System Engineers tend to associate high power systems with power electronics, it is worth noting that power systems related to nuclear fusion represent a challenging area rich in nonlinearities. Specifically, while nonlinear oscillations in power electronics are due to oscillations of electrical nature, the ones present in nuclear fusion can also refer to other physical quantities. We will refer to the latter taking into account macroscopic plasma instabilities affecting JET plasmas, and proposing both theoretical approaches and experimental ones to describe their dynamic. The former rely on nonlinear mathematical equations able to mimic the nonlinear behavior of the system under certain conditions while the latter are based on a physical realization of the system starting from its mathematical model.

High power systems related to power electronics are investigated in Chapter 2 where the importance of thermal modeling for the power electronics modules is pointed out and a new modeling strategy which starts from a distributed parameter analysis to obtain a lumped parameter model is introduced.

In this case, the proposed methodology is based on the assumption that the heat transfer problem can be assumed to be linear and the thermal impedances approaches can be therefore used. In this relevant case study nonlinearities in modeling high power systems can also be neglected under certain conditions. In particular, concerning high power modules, it is well-known how the geometry of the device and the proper choice of the cooling system can play a key role for these simplifications.

A data-driven approach based on neural networks to model plasma instabilities is presented in Chapter 3. This approach is introduced because physical models often require a deep knowledge of the system parameters that sometimes is difficult to obtain.

In Chapter 4 considerations and results on new identification methodologies based on parallel identification models for discrete-time systems are presented.

1

Introduction

In this chapter, we will focus on two main categories of high power systems presenting nonlinear oscillations: power electronics and experimental devices for the production of fusion energy. The former is characterized by nonlinear oscillations of electrical nature while in the latter oscillations of physical quantities of different natures are also present. The insurgence of nonlinear phenomena in these fields will be discussed in order to define the framework in which different modeling and identification approaches will be discussed in this thesis.

1.1 Nonlinear oscillation in power electronics

Speaking about high power devices or systems the first field that comes to the Systems Engineer's mind is the power electronics one. Actually nonlinear oscillations are present in high power systems of different natures. Power electronics, as one of the most representative field of high power systems, is of growing importance: it is estimated that during the twenty-first century more than 90% of the electrical energy generated in developed countries will be processed by power electronics before its final consumption [1]. Power electronic systems must be energy efficient and reliable, have a high power density thus reducing their size and weight, and be low cost to make the overall system economically feasible. High energy efficiency is important for several reasons: it lowers operating costs by avoiding the cost of wasted energy, contributes less to global warming, and reduces the need for cooling therefore increasing power density.

Power electronic systems are found in virtually every electronic device: DC/DC converters are used in most mobile devices (mobile phones, PDA etc.) to maintain the voltage at a fixed value whatever the voltage level of the battery is. These converters are also used for electronic isolation and power factor correction; AC/DC converters (rectifiers) are used every time an electronic device is connected to the mains (computer, television etc.). These may simply change AC to DC or can also change the voltage level as part of their operation; AC/AC converters are used to adapt either the voltage level or the frequency (international power adapters, light dimmer). In power distribution networks AC/AC converters may be used to exchange power between utility frequency 50 Hz and 60 Hz power grids; DC/AC converters (inverters) are used primarily in UPS or renewable energy systems or emergency lighting systems. When mains power is available, it will charge the DC

battery. If the mains fails, an inverter will be used to produce AC electricity at mains voltage from the DC battery.

The basic module of power electronic systems is then the converter. It utilizes semiconductor devices as switches and possibly energy storage elements such as inductors and capacitors. The presence of both types of component implies that the circuits are nonlinear, time-varying dynamical systems.

There are several unavoidable sources of unwanted nonlinearity in practical power electronics circuits [1]-[3]: the semiconductor switching devices (BJTs, MOSFETs, IGBTs, thyristors, diodes) have intrinsically nonlinear DC characteristics. They also have nonlinear capacitances and inductances. The control circuits usually involves nonlinear components such as comparators, PWMs, etc.

For all these reasons power converters are intrinsically nonlinear and can exhibit a variety of complex behaviors. Bifurcation theory has been applied successfully to simple models of power systems, and it has been shown that the theory of nonlinear dynamics can be used to explain undesirable low-frequency oscillation and voltage collapses [1]. This last phenomenon occurs because many power systems are forced to operate near their stability limits and thus they are vulnerable to perturbations of the operating conditions. So when these limits are exceeded, the system can exhibit undesired transient responses with the impossibility to retain a stable voltage profile [4].

Power electronics is increasingly being used to process power on a large scale so interconnected systems of converters are developing for high current, high power applications. In order to maximize the capacity and, to reduce the cost of existing power systems as demand rises, progressive interlinking is taking place on a continental level. In this case undesirable nonlinear effects can produce catastrophic bifurcations. On the other hand nonlinear phenomena in power electronics could provide benefits. In fact, in [5] it has been demonstrated the feasibility of using chaos to depress the spectral peaks of the interference from a switched mode power supply. In particular a boost converter (operating at a low switching frequency, 2.5 kHz) has been used to show that the spectrum of the input current is spread so its peaks are reduced and EMC is improved compared to the case when the circuit operates periodically. Moreover there was the advantage that this approach did not require extra circuitry compared with other spread spectrum techniques such as pseudo-random modulation and PWM.

It means that one possible area of application of nonlinear phenomena in power electronics is in reducing electromagnetic interference (EMI) in switch mode power supplies which are generators of both conducted (450 kHz to 30 MHz) and radiated (30 MHz to 1GHz) EMI. Therefore suppression of EMI is a major issue in switching-mode power converter design.

The first step in order to know how and how much nonlinear phenomena in power electronics could be dangerous or could bring benefits is to understand them. In many past studies the essential method to investigate nonlinear phenomena has been to obtain a discrete-time model of the systems under study and to analyze the observed phenomena in terms of the theory of bifurcations in maps developed by mathematicians and physicists. Several studies demonstrated that, when one parameter is varied while the others are kept fixed, the system behavior could change from periodic to chaotic [6]. The inherent sensitivity of chaotic systems to small perturbations may be exploited for synchronization and stabilizing limit sets such as unstable equilibriums or periodic orbits [7]-[10]. However, applications in power electronics are less obvious, because it is already possible to force large changes in behavior by means of active switching devices. In [11] it is shown that chaotic power converters may also be stabilized by appropriate feedback. From nonlinear dynamic systems theory it is know that in most chaotic systems there are periodic windows in the parameter space and a small inadvertent change of a parameter can bring the system out of chaos. It means ask themselves the question: Are we able to ensure reliable operation of a converter under chaos? This also begs another question: is there any point in making a power converter chaotic? Hamill conjectured that power electronics converter operating under chaos instead of a stable periodic orbit may have a better dynamic response, for instance in moving rapidly from one commanded output voltage to another [12].

In this direction Banarjee, Yorke, and Grebogi developed the theory of robust chaos [10] underlining the analytical conditions under which there would be no periodic window in a chaotic system and demonstrated that such a condition does occur in current mode controlled converters. Further studies are required to attack the problem in order to make use of the chaotic regime.

The growing interest in the chaotic behaviour that power converters can exhibit led to various methods for controlling chaos developed for power electronic circuits. Poddar, Chakrabarty, and Banerjee reported experimental control of chaos in the buck converter and the boost converter [6],[13]. In [14] Marrero, Font and Verghese observed that a potential advantage of using DC-DC converters in the chaotic regime is that the switching spectrum is flattened.

After a reasonable understanding of the nonlinear phenomena in power electronics is obtained the main question is: can we make engineering use of them?

The above mentioned works demonstrates that research in nonlinear phenomena of power electronics is going through an important phase of development. The past years of research, characterized by engineers that observed in power devices "strange" phenomena (e.g., chaos and bifurcation), helped the scientific community to focus and approach the topic in order to give an explanation to those "bad" laboratory observations. It seems that identification work will continue to be an important area of investigation. This is because power electronics emphasizes reliability and predictability, and it is crucial to understand the system behavior as thoroughly as possible and under all kind of operating conditions. Knowing when and how a certain bifurcation occurs will automatically means, for example, how to avoid it.

1.2 Nonlinear oscillations in nuclear fusion

Another relevant field related to high power systems is nuclear fusion [15]. Nuclear fusion is the process powering the Sun and stars. In the core of the Sun, at temperatures of 10-15 MK, Hydrogen is converted to Helium by fusion - providing enough energy to keep the Sun burning - and to sustain life on Earth.

A vigorous world-wide research programme is underway, aimed at harnessing fusion energy to produce electricity on Earth [16]. If successful, this will offer a viable alternative energy supply within the next 30-40 years - with significant environmental, supply and safety advantages over present energy sources.

To harness fusion on Earth, different, more efficient fusion reactions than those at work in the Sun are chosen by scientists, those between the two heavy forms of Hydrogen: Deuterium (D) and Tritium (T). All forms of Hydrogen contain one proton and one electron. Protium, the common form of Hydrogen has no neutrons, Deuterium has one neutron, and Tritium has two. If forced together, the Deuterium and Tritium nuclei fuse and then break apart to form a helium nucleus (two protons and two neutrons) and an uncharged neutron. The excess energy from the fusion reaction (released because the products of the reaction are bound together in a more stable way than the reactants) is mostly contained in the free neutron.

Fusion occurs at a sufficient rate only at very high energies on earth, and temperatures greater than 100 million Kelvin are required, as shown in Figure 1.1. At these extreme temperatures, the Deuterium - Tritium (D-T) gas mixture becomes a plasma (a hot, electrically charged gas). In a plasma, the atoms become separated - electrons have been stripped from the atomic nuclei (ions). For the positively charged ions to fuse, their temperature must be sufficient to overcome their natural charge repulsion.

In order to harness fusion energy, scientists and engineers are learning how to control very high temperature plasmas. The adoption of much lower temperature plasmas are now widely used in industry, especially for semi-conductor manufacture. However, the control of high temperature fusion plasmas presents several major science and engineering challenges - how to heat a plasma to in excess of 100 MK and how to confine such a plasma, sustaining it so that the fusion reaction can become established.

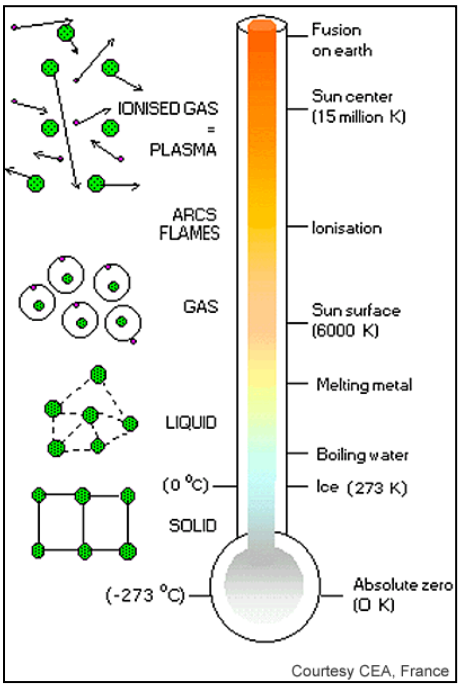

Figure 1.1: Temperature needed for plasma on Earth (>10^7 K)

Three parameters (plasma temperature, density and confinement time) need to be simultaneously achieved for sustained fusion to occur in a plasma. The product of these is called the fusion (or triple) product and, for D-T fusion to occur, this product has to exceed a certain quantity - derived from the so-called Lawson Criterion after British scientist John Lawson who formulated it in 1955. Attaining conditions to satisfy the Lawson criterion ensures the plasma exceeds Breakeven - the point where the fusion power out exceeds the power required to heat and sustain the plasma. Fusion reactions occur at a sufficient rate only at very high temperatures - when the positively charged plasma ions can overcome their natural repulsive forces.

Typically, in JET, over 100 MK is needed for the Deuterium-Tritium reaction to occur - other fusion reactions (e.g. D-D, D-He3) require even higher temperatures. The number of fusion reactions per unit volume is roughly proportional to the square of the density. Therefore the density of fuel ions must be sufficiently large for fusion reactions to take place at the required rate. The fusion power generated is reduced if the fuel is diluted by impurity atoms or by the accumulation of Helium ions from the fusion reaction itself. As fuel ions are burnt in the fusion process they must be replaced by new fuel and the Helium products (the "ash") must be removed. The Energy Confinement Time is a measure of how long the energy in the plasma is retained before being lost. It is defined as the ratio of the thermal energy contained in the plasma and the power input required to maintain these conditions. On JET magnetic fields are used to isolate the very hot plasmas from the relatively cold vessel walls in order to retain the energy for as long as possible. A significant

fraction of losses in a magnetically-confined plasma is due to radiation. The confinement time increases dramatically with plasma size (large volumes retain heat much better than small volumes)- the ultimate example being the Sun whose energy confinement time is massive.

For sustained fusion to occur, the following plasma conditions need to be maintained (simultaneously):

- ✓ plasma temperature: (T) 100-200 MK;
- ✓ energy confinement time: (t) 4-6 s;
- ✓ central density in plasma: (n) 1-2 x 1020 particles m-3 (approx. 1/1000 gm-3, i.e. one millionth of the density of air). Note that at higher plasma densities the required confinement time will be shorter but it is very challenging to achieve higher plasma densities in realistic magnetic fields.

Since a plasma comprises charged particles: ions (positive) and electrons (negative), powerful magnetic fields can be used to isolate the plasma from the walls of the containment vessel - thus enabling the plasma to be heated to temperatures in excess of 100 MK. This isolation of the plasma reduces the conductive heat loss through the vessel and also minimizes the release of impurities from the vessel walls into the plasma that would contaminate and further cool the plasma by radiation. In a magnetic field the charged plasma particles are forced to spiral along the magnetic field lines (Figure 1.2).

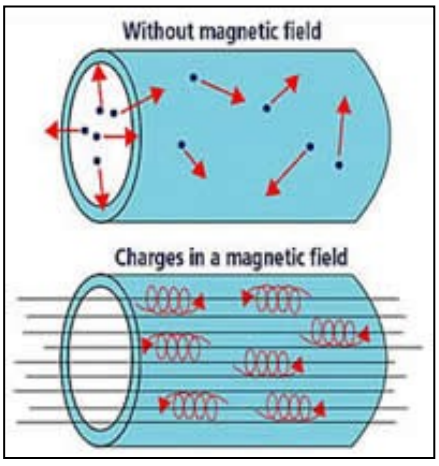

Figure 1.2: Trajectories of plasma ions

The most promising magnetic confinement systems are toroidal (from torus: ring-shaped) and, among these, the most advanced is the Tokamak. Currently, JET is the largest Tokamak in the world although the future ITER machine will be even larger.

Other, non magnetic plasma confinement systems are being investigated - notably laser-induced inertial confinement fusion systems [17].

In a Tokamak the plasma is heated in a ring-shaped vessel (or torus) and kept away from the vessel walls by applied magnetic fields. The basic components of the Tokamak's magnetic confinement system are :

- the toroidal field - which produces a field around the torus. This is maintained by magnetic field coils surrounding the vacuum vessel (see Figure 1.3);
- the poloidal field - which produces a field around the plasma cross section. It pinches the plasma away from the walls and confines the plasma. The poloidal field is induced both internally, by the current driven in the plasma (one of the plasma heating mechanisms) and, externally, by coils that are positioned around the perimeter of the vessel.

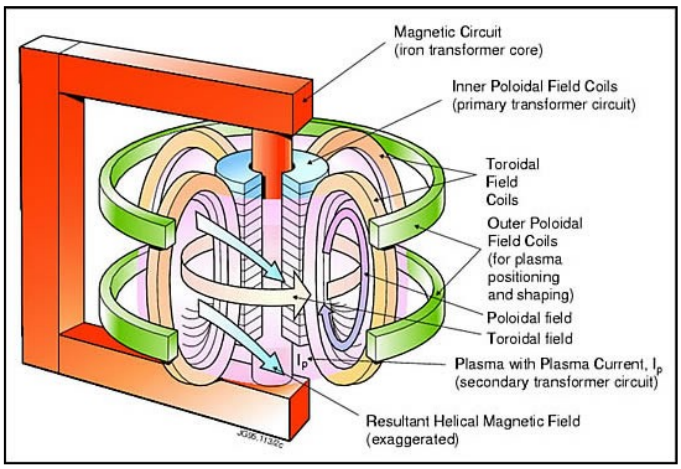

Figure 1.3: Toroidal and poloidal coil in JET's Tokamak

The main plasma current is induced in the plasma by the action of a large transformer. A changing current in the primary winding or solenoid (a multi turn coil wound onto a large iron core in JET) induces a powerful current (up to 5 MA on JET) in the plasma - which acts as the transformer secondary circuit. A simplified cutaway diagram of JET's Tokamak is shown in Figure 1.4.

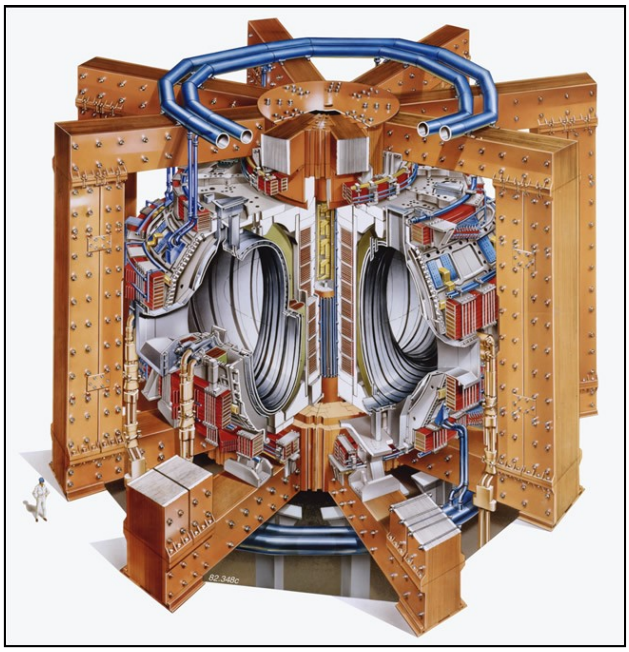

Figure 1.4: Simplified cutaway diagram of JET's Tokamak.

Securing future energy supply is the major challenge for Europe and the world. Global energy demand will increase over the next years as people in developing countries become wealthier. Energy sources using renewable technologies such as wind power will be necessary to satisfy future needs, but the strong energy demand leads us to develop new energy sources that can provide continuous, large-scale power for the long term without harming the environment. Fusion energy could represents a potential solution in this direction. Joint European Torus (JET), the major experiment of the European Union fusion research programme [18], has allowed studies of tokamak plasmas up to reactor relevant performance and to resolve key physics and engineering issues for the design of the International Tokamak Experimental Reactor (ITER).

Every individual plasma experiment at JET (pulse) lasts several tens of seconds and during experimental campaigns there are several pulses a day. Therefore power supplies are designed to supply pulsed loads. Each JET pulse consumes around 10GJ of energy [18]. More than 50% of this power and energy is taken by the British 400kV Grid. It means that magnetic fusion experiments require extensive use of AC/DC conversion systems: semiconductors such as diodes and thyristors must be used to convert the grid AC power into a dynamic DC form suitable for JET. (The rest of power is taken by two local flywheel generators with diode converter). A key role in the success of JET has been the development of power conversion systems, which supplies the main electrical loads of a tokamak. European countries are not the only could give a contribute to ITER development. Advanced studies in order to improve tokamaks power conversion systems are taking

place in other countries of the world: in China innovative power supply systems for EAST Superconducting tokamak are continually evolving and could represent a testbed for the technologies proposed for ITER project [19]. On the one hand power electronics plays, once again, a key role in JET Tokamak because nonlinear phenomena are present in tokamaks power conversion systems. On the other hand, Tokamaks are also characterized by nonlinear oscillations of different nature [15]. Specifically, tokamak plasmas are affected by a series of instabilities, which can play an important role on the performance of the plant and even compromise the correct operation of experiments. A lot of progress has been achieved in the last decades to understand the main causes of these instabilities but various aspect of their dynamics remain not completely understood. Edge Localized Modes (ELMs) are instabilities that appear when the plasma is in the high confinement mode H-mode configuration. The higher plasma energy in these configurations is partly due to a "pedestal" at the edge of the pressure profile. This pedestal results from pedestals on both the density and temperature profiles. While it is obvious that the pedestal is advantageous to achieve higher confinement, the price is paid by the inevitable steep gradients at the plasma edge which leads to instabilities – the ELMs [15].

One of the main macroscopic modes in a Tokamak is the sawtooth instability which is present over a wide range of operating conditions. This is observed as a relaxation oscillation in the centre of the plasma, which appears most clearly in the time evolution of the electron temperature, derived from the Electron Cyclotron Emission on JET. The clear signature is sawtooth-like behaviour of the time series waveform in the central region of the plasma, with inverted behaviour in the outer region. The abrupt collapse of the temperature is attributed to a central, helical instability which causes the expulsion of particles and energy, detected as a heating pulse propagating in the outer region. On the plasma with high κ (density), we can observe a synchronization between ELMs and Te (electron temperature) sawteeth. When temperature collapses, an ELM can be triggered. This phenomenon is due to energy that goes from core to edge plasma. The pressure gradient becomes too important and the plasma edge loses confinement. The signature of the ELMs is very clear on the electron temperature and on the magnetic field, as measured with the pick up coils. ELMs can be also identified by Dα radiation (visible radiation emitted by excited atoms of deuterium fuel). An explicit example in Figure 1.5 shows clearly the interaction between ELMs on Dα and sawteeth on electron temperature.

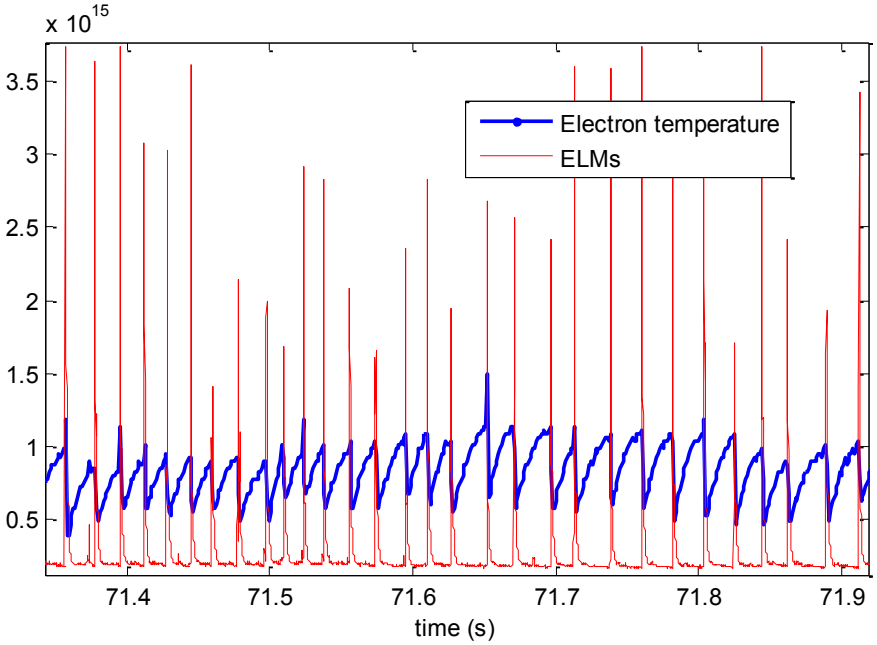

Figure 1.5: Interaction between electron temperature (blue) sawteeth and ELMs (red) visible on Dα radiation for experiment (pulse) #50722.

There are three categories of ELMs [15]:

- Type I ELMs are essentially giant ELMs. This type is particular threat because of the large heat loss pulse involved and the consequent unacceptably high heat load on the divertor.
- Type II ELMs are intermediate category which avoid the heat pulse of type I but do not lead a severe loss of general confinement.
- Type III ELMs are continuous grassy ELMs which are associated with a substantial deterioration of confinement.

1.2.1 Modeling plasma instabilities by using theoretical approaches

Particular attention has been given to the modeling of instabilities rising evident macroscopic implications, such as ELMs, sawtooth and Neoclassical Tearing Modes. Models can be derived from experimental observations, by means of data fitting or neural networks approximations [20], or applying approaches based on geometrical consideration exploiting the peculiar characteristics of the reactor. An example of the first approach is based on neural networks for modeling ELMs and sawtooth instabilities [20], while an example of the second approach can be found in [21] where a nonlinear gross behavior model for tokamak plasmas has been introduced starting from symmetry considerations. This ideal nonlinear model is essentially based on the relatively simple application of the equivariant bifurcation theory and it is able to reproduce the principal qualitative characteristics of ohmically heated tokamak discharges. Following [21], let us consider some simplificative hypotheses on tokamak geometry. A realistic geometric approximation is to consider the tokamak as a periodic cylinder. Thanks to this simplification the simplest realistic nonlinear model satisfying rotational simmetry constraints can be described considering the generic unstable modes of amplitude $a(t)$ with an angular coordinate φ, so that the solution may be written as:

$$y = ae^{jn\varphi} + \bar{a}e^{-jn\varphi} \qquad (1.1)$$

where n is the integer mode number and the $\bar{a}$ denotes the complex conjugate. If the dynamics of the mode is ideal (Lagrangian), imposing invariance under rotation we obtain the following equation:

$$\ddot{a} = \gamma a + 2\mu a^3 \qquad (1.2)$$

Equation (1.2) can be rewritten as the following system of two first-order differential equations:

$$\begin{cases} \dot{x} = y \\ \dot{y} = \gamma x + 2\mu x^3 \end{cases} \qquad (1.3)$$

The dynamic characteristics of model (1.3) allows to mimic two important peculiarities of tokamak plasmas, i.e. the occurrence of saturated traveling waves and the bursty and sawtoothing behavior. This makes the model suitable for fitting real data acquired during experiments in which the occurrence of ELMs and sawtooth can be observed. Furthermore, quantitative information regarding the nonlinear terms in the real experiment can be useful to derive a more accurate model. An example of bursty oscillations is shown in Figure 1.6 in which the solution of the system (1.3) is obtained for $\gamma = 1,\ 2\mu = -1,$ initial conditions $x(0) = 0.01$ and $y(0) = 0$.

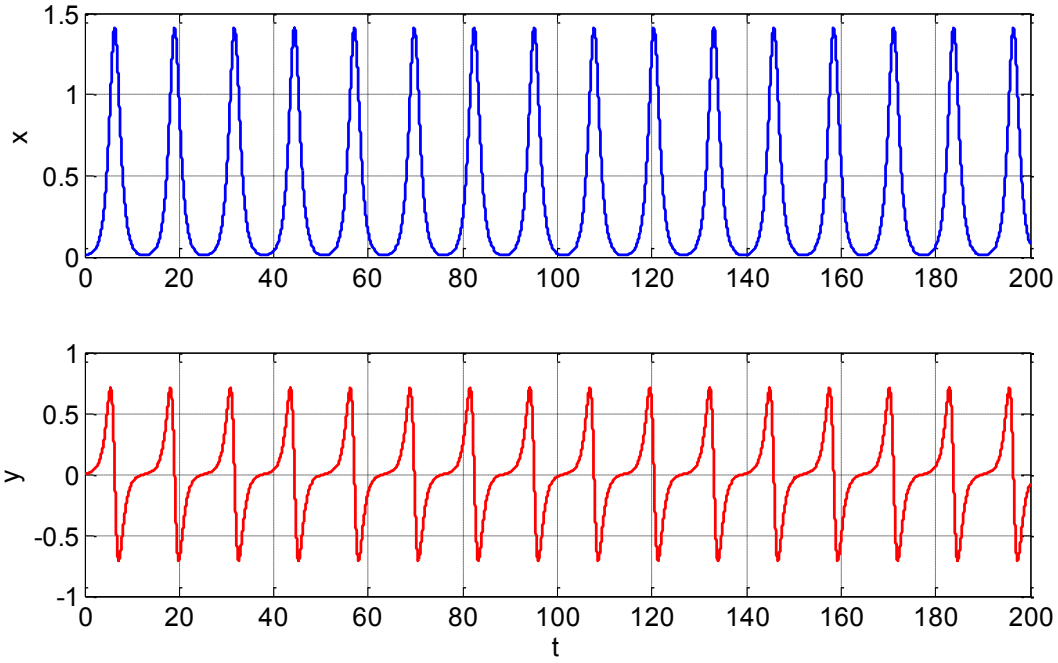

Figure 1.6: Solutions of the system (1.3) for $\gamma = 1,\ 2\mu = -1$ and initial conditions $x(0) = 0.01$, $y(0) = 0$.

1.2.2 Modeling plasma of instabilities by using experimental approaches

Although the dynamics of nonlinear systems can be studied by using numerical simulations, in some cases the particular characteristics of the considered system suggest to investigate it also in presence of non ideal conditions, e.g. considering an experimental approach based on electronic analogue [22]. In fact, an electronic circuit, designed starting from the mathematical model of a dynamical system, can be easily implemented and its behavior can be characterized observing the electrical waveform generated by the circuit itself. Especially in presence of parameters which can lead to bifurcations, the behavior of the system can be more rapidly investigated with such experimental approach. The parameter values are designed applying the harmonic balance principle [23] in order to derive the conditions allowing the observation of the onset of stable nonlinear oscillations. The model introduced represents a generalization of the conservative analytical model (1.3) obtained introducing dissipative terms. The considered model is then of interest in the field of modeling physical phenomena as it represents the generalization of the plasma gross behavior model. Let us consider the following dynamical system:

$$\begin{cases} \dot{x} = y + ax \\ \dot{y} = \gamma x + by - Rf(x, \dot{x}) \end{cases} \qquad (1.4)$$

where a, b, γ and R are design parameters and $f(x, \dot{x}) = x^3 + \delta x^2 \dot{x}$ is a nonlinear functional. The system in Eqs (1.4) represents a nonlinear oscillator with dissipative terms and a cubic nonlinearity involving a derivative term. In order to obtain stable oscillations, system parameters can be designed following the harmonic balance approach based on the describing function (DF) approximation [24]. The analysis based on the harmonic balance method allows to identify whether or not a limit cycle $y_0(t) = Asin(\omega t) + B$ is a stable solution for the considered system, provided that it has been rewritten in the so-called Lur'e form. Lur'e systems are nonlinear systems of the simplest architecture formed by a dynamical part $G(s)$ and a feedback nonlinear part N as shown in Figure 1.7.

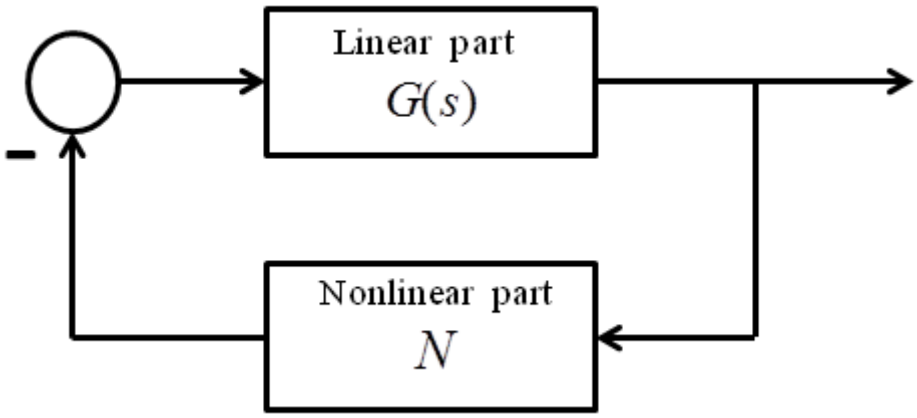

Figure 1.7: Lur'e system block diagram.

More in detail the nonlinearity N can be approximated with the corresponding static and dynamic describing function [25] N_0 and N_1, where the amplitude A and the bias B of y_0 can be derived solving the equations:

$$\begin{aligned} 1 + G(0)N_0(A, B) &= 0 \\ 1 + G(j\omega)N_1(A, B, \omega) &= 0 \end{aligned} \qquad (1.5)$$

where $G(s)$ has been considered for $s = j\omega$. Solving Eqs. (1.5) means to express A as a function $A(B)$ from the static equation and the to consider the intersections between the curve $G(j\omega)$ and the curve $-1/N_1(A(B), B)$ in the complex plane. At each intersection corresponds a limit cycle with a given frequency, amplitude, and bias level. The stability of the predicted limit cycle can be inferred

applying the Loeb criterion [26]: if the points near the intersection along the curve $-1/N_1(A(B),B)$ for increasing values of B are not encircled by the curve $G(j\omega)$, then the limit cycle is stable. The system in Eqs (1.4) can be rewritten according to the Lur'e form as the following second-order differential equation:

$$\ddot{x} - q\dot{x} + px = -R(x^3 - \delta x^2 \dot{x}) \qquad (1.6)$$

where $y = \dot{x}, p = \gamma - ab$, and $q = -(a+b)$. The linear part of the oscillator is described by the transfer function $G(s) = \dfrac{R}{s^2 - qs + p}$, while the dynamic nonlinearity $f(x) = x^3 - \delta x^2 \dot{x}$ can be approximated by the following static and dynamic describing functions:

$$\begin{aligned} N_0(A,B) &= \frac{1}{2}(3A^2 + 2B^2) \\ N_1(A,B,\omega) &= \frac{3}{4}(A^2 + 4B^2) - j\frac{1}{4}\delta\omega(A^2 + 4B^2) \end{aligned} \qquad (1.7)$$

Substituting Eqs. (1.7) in (1.5), a unique solution $y(t) = Asin(\omega t) + B$ can be found with $A = \dfrac{2}{5R}\sqrt{5(\dfrac{Rq}{\delta} - Rp)}$, $B = \dfrac{\sqrt{5(9Rp + 18Rq^2 + Rp^2\delta^2 - \frac{54Rq}{\delta} - 9Rpq\delta)}}{5R(p\delta^2 - 3q\delta + 9)}$, and $\omega = \sqrt{p - \dfrac{3q}{\delta}}$.

Hereinafter, the uniqueness of the limit cycle with respect to a given set of parameters will be exploited in order to design and implement a circuital analogue of the proposed oscillator. At this point, the aim of is to design a circuital implementation of the nonlinear model in Eqs. (1.4). Let us consider the circuit's schematic reported in Figure 1.8

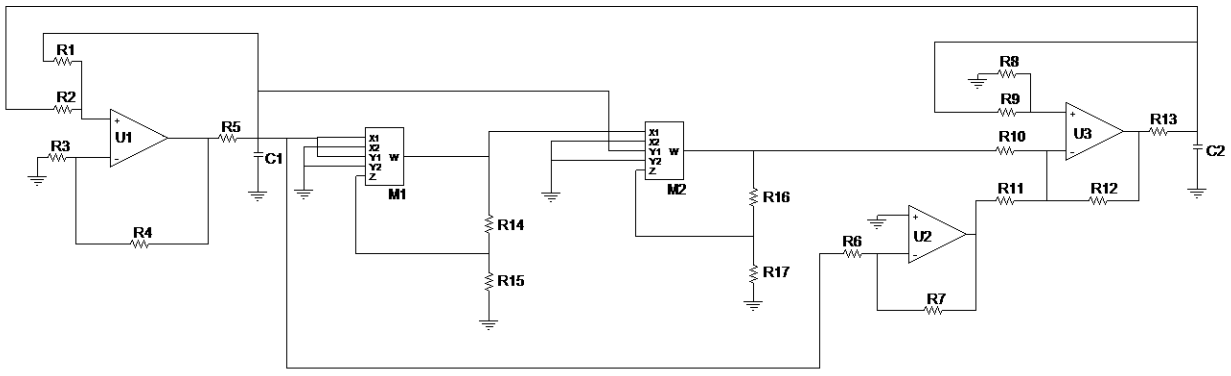

Figure 1.8: Circuit implementing system in Eqs. (1.3)

It has been designed following the state variable approach [27], hence the circuital equations governing the circuit are:

$$\begin{cases} \frac{dX}{d\tau} = \frac{1}{R_5 C_1}\left[\frac{R_2}{R_1+R_2}\left(1+\frac{R_4}{R_3}\right)X + \frac{R_1}{R_1+R_2}\left(1+\frac{R_4}{R_3}\right)Y - X\right] \\ \frac{dY}{d\tau} = \frac{1}{R_{13} C_2}\left\{\left[\frac{R_8}{R_8+R_9}\left(1+\frac{R_{12}(R_{10}+R_{11})}{R_{10}R_{11}}\right)\right]Y - \frac{R_{12}}{R_{10}}F(x) + \frac{R_7 R_{12}}{R_6 R_{11}}X - Y\right\} \end{cases} \quad (1.8)$$

OP-AMPs U1 and U3 implement an active integrator made by a passive RC group and an algebraic adder, the two cascaded multipliers M1 and M2 realize the cubic nonlinearity F(x) while OP-AMP U2 allows to set parameter γ. Even if the circuit is designed in order to compensate the dissipative terms involved in the integrators transfer function, dissipative effects cannot be completely avoided due to tolerances in circuital components. This means that a and b are small but different from zero. Furthermore, a temporal scaling $\tau = \kappa t$ has to be introduced to make signals frequency compatible with analog circuitry. We fixed $\kappa = \frac{1}{R_5 C_1} = \frac{1}{R_{13} C_2} = 20000$.

Although the nonlinear block should realize a cubic nonlinearity, the actual nonlinearity is of the form considered in Eqs. (1.4). According to [28], the model of the analog multiplier based on [29] involve further terms, in which the multiplication between the input and its derivative appears, whose coefficients are functions of the frequency of the input signal. In order to evaluate these coefficients, let us start from the assumption that the maximum signal frequency is sufficiently small, so that the higher order derivatives of the output signal can be neglected, the model of the single multiplier realizing the square term can be written as:

$$x_{mult}^2 = K(x^2 - 2T_a x\dot{x}) \quad (1.9)$$

The parameters K and T_a can be estimated by applying a DC voltage at one of the input ports and a sinusoidal sweep signal at the other input port. Measuring the zero-frequency values of the voltage gain and the group delay relative to the AC signals using an AD633 multiplier at the time-scale of the circuit, $K = 0.9986$ and $T_a = 1.6012\mu s$ have been identified. Thus the model of the two cascaded multipliers is given by:

$$x_{mult}^3 = K^2[x x_{mult}^2 - T_a(\dot{x} x_{mult}^2 + x\dot{x}_{mult}^2)] \quad (1.10)$$

By expanding products in (1.10) and neglecting the T_a^2 terms the model can be rewritten as follow:

$$x_{mult}^3 = K^2 x^3 + (4K^2 T_a + K T_a) x^2 \dot{x} \quad (1.11)$$

obtaining a value for parameter $\delta = \frac{1}{R_{13}C_2}.(4K^2T_a + KT_a) \approx 0.1592$. The circuit parameters of Figure 1.8 are chosen so that equations (1.8) match equations (1.2) with: $R_1 = R_3 = 108.69k\Omega$, $R_2 = R_4 = R_7 = R_{11} = R_{12} = 100k\Omega$, $R_5 = R_{13} = 5k\Omega$, $R_6 = 108.69k\Omega$ (potentiometer), $R_8 = 45.54k\Omega, R_9 = 106.38k\Omega, R_{14} = R_{16} = 1k\Omega, R_{15} = R_{17} = 9k\Omega$, $C_1 = C_2 = 10nF$. In this case, the values of parameters can be identified as $p = -0.9146$, $q = -0.1422$, and $R = 0.9835$. The harmonic balance method allows to determine the unique stable solution of Eqs.(1.7) as shown in Figure 1.9.

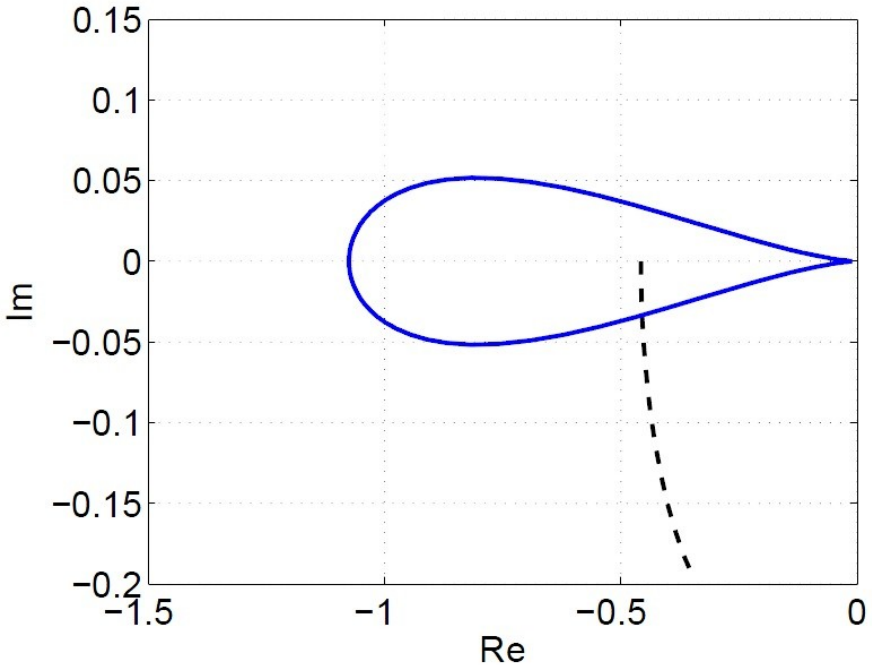

Figure 1.9. Plot of $G(s)$ (blue line) and $-1/N_1(A(B), B)$ (black dashed line) in the complex plane for the parameter values implemented in the circuit.

The circuit, shown in Figure 1.10, has been implemented with off-the-shelf components and then analysed by acquiring the waveforms generated.

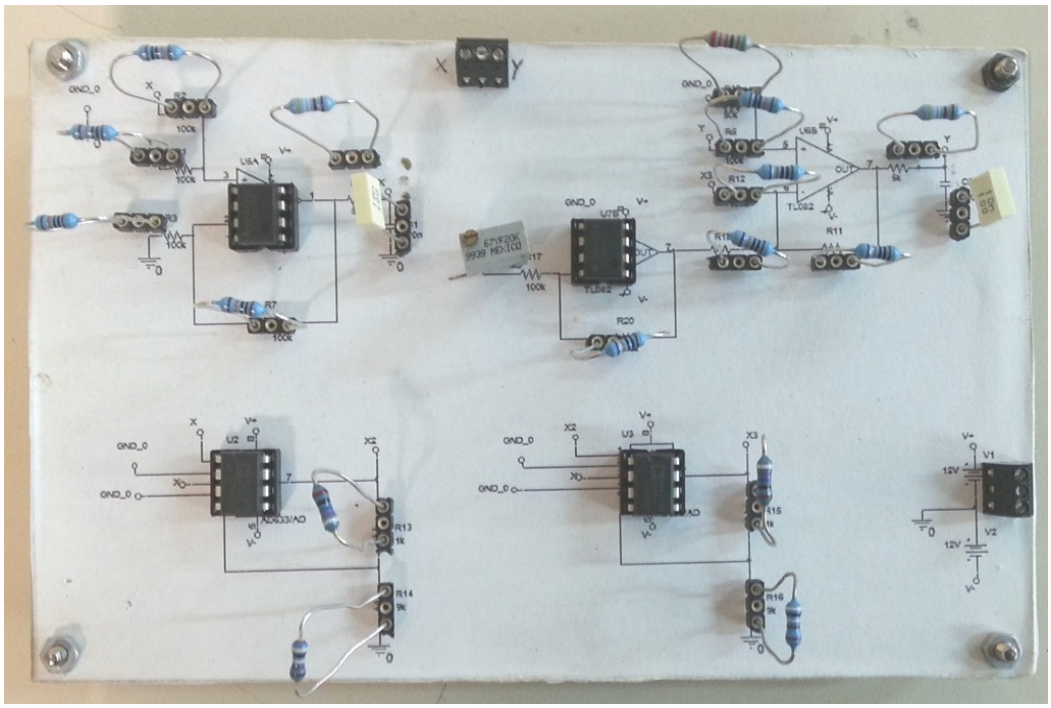

Figure 1.10: Circuit implementing system in Eqs. 1.3

The dataset shown in Figure 1.11 has been acquired by using a National Instruments (NI-USB6251) data acquisition board with a sampling frequency $f_s = 70kHz$, and represents the limit cycle shown by the circuit when $\gamma = 0.9$. Furthermore, the behavior of the circuit with respect to system parameter γ has been studied. According to the harmonic balance theory, the frequency of the limit cycle is directly dependent on $p = \gamma - ab$, and, in fact, this relationship can be observed on the frequency of the limit cycle for increasing values of γ, as shown in Figure 1.12.

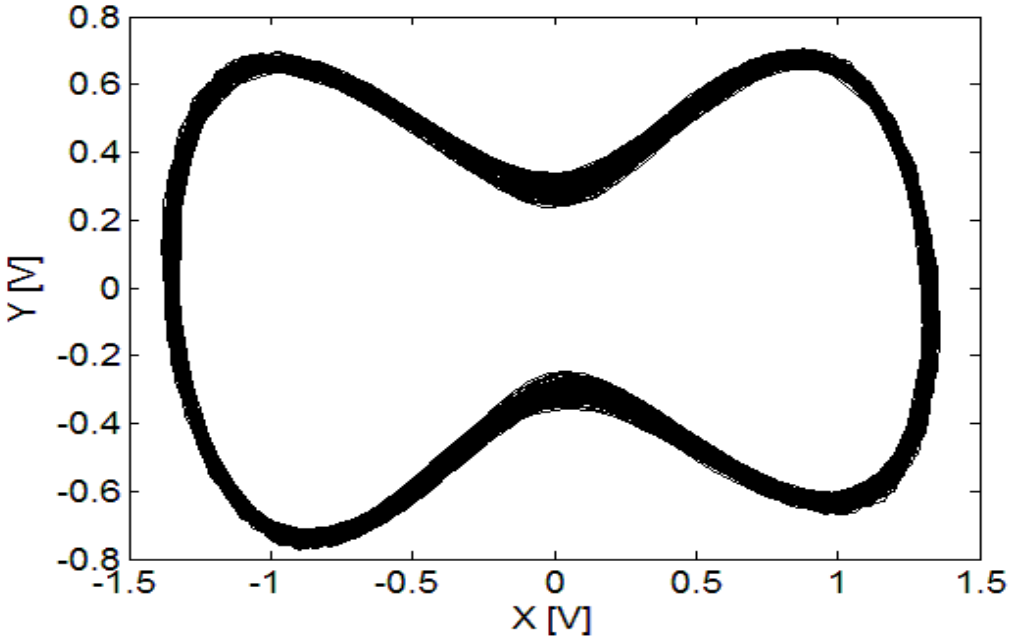

Figure 1.11: Limit cycle shown by the nonlinear circuit for $\gamma = 0.9$

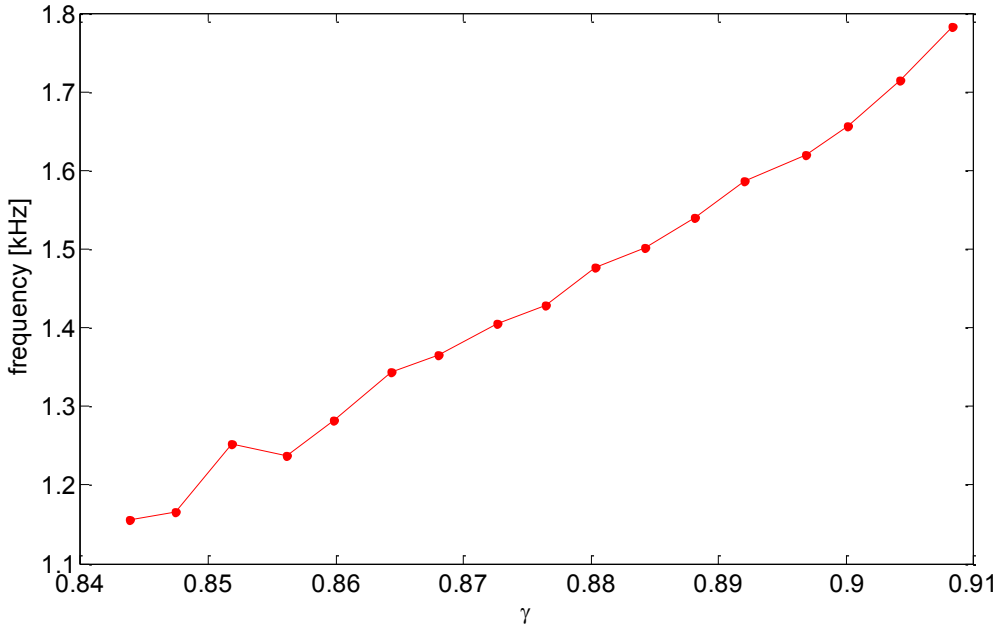

Figure 1.12: Frequency of the limit cycle shown by the circuit as a function of γ.

The model proposed above has important features which make it suitable for representing the behavior of Tokamak plasmas affected by several macroscopic and microscopic instabilities whose

interactions are essentially nonlinear [15]. The model in Eq. (1.3) is the conservative representation of the system considered. Under this perspective, the circuital analogue presented can be used in assisting the refinement of models for the nonlinear behavior of oscillations in presence of plasma instabilities exploiting approaches based on synchronization [30].

1.2.3 Remarks on modeling of high power systems

The study discussed in the previous section underlines the importance to build the model of the high power system in order to characterize its nonlinear oscillations. More in general, the characteristics of the power devices require the definition of new identification strategies to work alongside the existing ones. According to our analysis the following emerging issues may be identified.

- The need of make use of multi-physics techniques by integrating distributed parameters modeling strategies and lumped parameter ones. Power devices have traditionally been modeled using 3D field solvers based on the finite element method (FEM). This approach, which can be described as physical modeling, entails decomposing the device/system geometry into a collection of volume or surface elements (meshing), and then solving a system of partial differential equations for the field values at the element control points. The use of multi-physics field solver allows the designer to investigate on the presence of nonlinearities of different nature. Specifically, for high power systems/modules it is of relevant importance the study of thermal aspects to ensure the reliability of the device itself that is subject to strong thermal constraints. However, often, FE modeling requires an high computational cost and for this reason the need arises to integrate it with lumped parameters modeling strategies that allow a fast simulation of the system/device. Particularly, in the thermal domain, this integration is possible by designing passive electrical networks reproducing the thermal behavior of the system/device. In Chapter 2 a new modeling methodology related to this approach has been proposed.

- The need of nonlinear models that rely on data-driven approaches to identify nonlinearities in high power systems. This is due the fact that physical models require a detailed knowledge of the device/system physics parameters that are often difficult to find. A neural network approach based on the identification of dynamical equations from data in Nuclear Fusion is presented in Chapter 3.

- The need to investigate on new identification methodologies based on parallel identification models to reproduce the system behavior. Specifically the approaches based on parallel identification models are more powerful than simple series parallel identification model (predictor)

that require the continuous measurement of the state of the plant. In Chapter 4 an investigation on this techniques based on adaptive control is proposed.

2

Thermal modeling of high power modules

Power electronic modules are realized by integrating several semiconductor chips inside one package. In this chapter, a new thermal modeling procedure and its application to a power electronic module are presented [31]. The adopted modeling strategy consists of the derivation of numerical thermal impedances by 3D Finite Element (FE) models, validated by comparison with available experimental data, and of the coefficients identification of the RC passive network, through a specific topology, here introduced, to obtain a lumped parameter model of the thermal behavior of the module.

2.1 Thermal modeling

The growing demand for high power devices concentrated in small volumes is driving the industrial research towards the design of integrated power modules [32],[33]. They are realized by integrating several chips (IGBT, diodes, MOSFET) inside one package. This causes high power density that produces strong thermal constraints on the package. Furthermore, the different chips included in the device are thermally coupled, so that the thermal power generated by one chip causes the heating of both that chip and all the others in the package. Thermal aspects become dominant and strongly influence both the module working conditions and its lifetime. As a result, the probability of failure due to the thermal stress significantly increases, thus impacting on the reliability [34]-[36]. In order to keep the devices in safe operating conditions, the silicon chips junction temperature (both in transient and in steady-state regime) should be controlled. On the one hand, thermal simulators need to be more and more capable to reproduce the device thermal behavior. On the other hand, if more than just a few chips need to be thermally modeled, the simulation time of three-dimensional models increases enormously. A trade-off is therefore necessary. This study addresses the problem of reproducing the thermal behavior of high power modules by means of equivalent circuit models. Many papers describing numerical methods for thermal analyses of multichip power modules have been published [34]-[45]. Two main strategies are proposed in the literature to model the thermal behavior of a power electronic module. The first one, is a distributed parameter approach [37]-[41],[46] relying on the underlying physical mechanisms of the devices to develop a system of equations that fully describes the system response on the thermal domain. The system of equations can be solved employing different numerical methods, such as the Finite Element Method (FEM)

[37],[39]-[41],[46] and the Boundary Element Method (BEM) [38]. The second one, called lumped parameters approach, reproduces the thermal behavior of the semiconductor components by deriving a thermal equivalent circuit or by using an analytical expression able to assess the thermal response of the system [42]-[44]. Both approaches lead to the derivation of thermal impedances, which represent in a concise way the thermal response of the module, at selected locations of the device. The Foster type network topology is generally proposed in the literature [42] to reproduce the behavior of both thermal self impedances and mutual impedances. Other strategies for lumped parameters modeling rely on mathematical relations to fit the thermal mutual impedance to address this problem [37].

The novelty of the proposed approach can be essentially summarized in the following points: 1) to have adopted an integrated procedure starting from FE models validated by experimental data; 2) to have introduced a new topology for the equivalent RC network used to model the thermal response of the system. The proposed topology allows to model large delays which are observed for mutual thermal impedances. The procedure is tailored on a new power module fabricated by STMicroelectronics that required a specific investigation design tool. The proposed modeling strategy consists of different steps. Firstly, a thermal 3D FE model has been derived and validated by comparison with experimental data. Then, the thermal impedances extracted from the FE model, have been reproduced by means of passive circuit topologies whose parameters are identified using optimization algorithms. Thermal data, collected by measurements or FE simulations, can be used for modeling in an electrical circuit simulator, if an electrical equivalent network whose step response describes the transient thermal impedance is available. Although the idea of finite element analysis and equivalent circuits is not new, the typical passive network topologies used to address this problem (Foster and Cauer networks) have significant limitations in accurately representing thermal mutual impedances. In this paper an electrical passive network topology is presented to emulate the transient mutual impedances which are characterized by slow transients. More specifically, the relevant quantity used to estimate the transfer function is the temperature response from the output port of the equivalent circuit. As explained in Section 2.3, thermal mutual impedances are often characterized by a time delay depending on the chips mutual position inside the package. The proposed passive network topology is able to properly reproduce both the thermal impedances transient behavior and their steady state regime.

2.2 A new integrated procedure for power electronic modules

The methodology introduced to characterize the thermal behavior of a power module consists of different steps shown in Figure 2.1. The first step is to collect thermal data. Thermal impedances waveform can be obtained from both a FE model or experimental data (FE Model/Experimental Characterization). The FE model allows to obtain the spatial distribution of temperature, while experimental data are usually related to temperature information at some critical points (Thermal Data). Once thermal impedances are available, the next step of the procedure is the choice of the model. In particular, the model structure is fixed (as discussed in Section III), while the order N of the system has to be selected. This step is indicated as choice of the RC equivalent model. The circuit parameters are identified by using optimization techniques based on the Nelder-Mead simplex method which minimizes the error between the thermal impedance provided by the network and the one extracted from the FE model or from experimental data (Parameters Identification). At this point it is possible to check whether the chosen order N of the equivalent RC network suffices to properly fit the thermal impedances (Validation stage). If the order N is not able to ensure a good fit, the procedure steps back to the choice of the order of the equivalent RC model. The last step of the developed procedure consists of performing the fast simulation of the whole module thermal behavior by means of a generic circuit simulator (Fast Simulation of thermal behavior). As mentioned above, two different approaches may be adopted to extract the thermal behavior of the module. In the proposed approach, thermal data have been generated by numerical models built-up exploiting the COMSOL Multiphysics software, a commercial FE-based software able to solve both partial and ordinary differential equations.

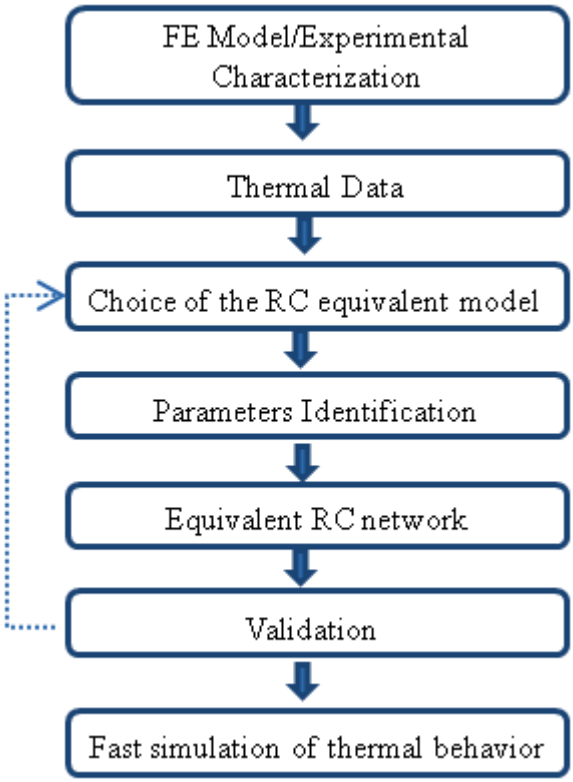

Figure 2.1: Flow Diagram of the proposed methodology.

The heat conduction equation describing the temperature field in the computational domains is [47]:

$$\nabla^2 T + \frac{\dot{g}}{\lambda} = \frac{1}{k}\frac{\partial T}{\partial t} \qquad (2.1)$$

where T represents the temperature, k the thermal diffusivity, λ is the thermal conductivity and ġ the volumetric heat generation. Eq (2.1) is solved by using the FE method, mainly consisting in the discretization of the continuous equations on the physical computational domains by means of chosen numerical elementary entities, i.e. the finite elements. This step allows the partial differential equation to turn into an algebraic system of equations, which is solved applying the unsymmetric multifrontal package direct solver [48]. Once initial and boundary conditions are assigned, the solution can be computed and gathered in terms of temperature distribution all over the module. Typically, power modules are made by thin vertical layers and have large horizontal dimensions. It means that the heat flux predominantly flows from the top to the bottom of the module. Therefore, the flux through the lateral sides can be neglected, and adiabatic constraint can be assumed as the boundary condition. A properly designed heat sink allows to dissipate the whole

heat generated; then, the baseplate's bottom side can be assumed as an isothermal surface. In these conditions the heat transfer problem can be assumed to be linear [37],[45] and this approximation finds good agreement with most of the power electronic applications. Under this hypothesis, the superposition principle can be used. The thermal behavior of the module may be therefore obtained by assuming, at each time, only one device acting as a heat source and evaluating the temperature along the module. The procedure is then repeated for each device of the module and the results added to obtain the complete thermal response. In particular, a power pulse (P_i) is applied only on a single chip and then the thermal responses on all chips are obtained. The temperature of the bottom side of the baseplate is called reference temperature (T_r). The approach is schematically shown in Figure 2.2. More specifically, the input power is applied as a surface power density uniformly distributed on the chip top surface equivalent to a power of $P_i = 1W$. The reference temperature is $T_r = 25$ °C.

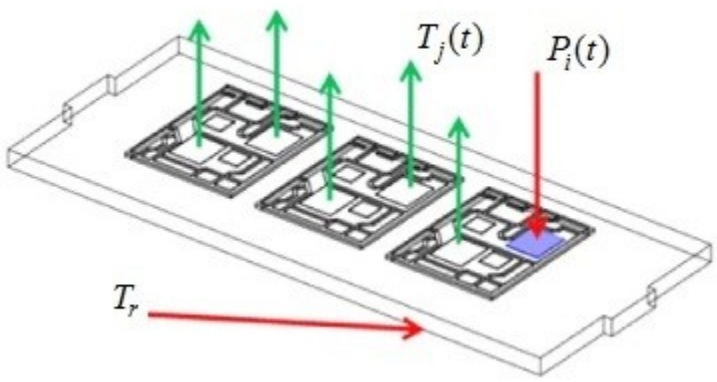

Figure 2.2: Approach used to evaluate thermal responses on the different chips of the module.

To characterize the thermal response of all chips, the generic thermal impedance is defined as:

$$z_{th,ij} = \frac{T_{ij} - T_r}{P_j} \quad (2.2)$$

where P_j is the power applied on chip j and T_{ij} is the temperature on the centre of the chip i top area, when chip j is heated. If $i = j$ the response $z_{th,ii}$ is named thermal self impedance while if $i \neq j$ the resulting $z_{th,ij}$ is named thermal mutual impedance and represents the thermal coupling effect between the two considered devices. Then, for a module having n devices, it is possible to assemble the following matrix of thermal impedances:

$$z_{th} = \begin{pmatrix} z_{th,1,1} & \cdots & z_{th,1,n} \\ \vdots & \ddots & \vdots \\ z_{th,n,1} & \cdots & z_{th,n,n} \end{pmatrix} \quad (2.3)$$

in which the entries in the main diagonal are the self impedances of each chip while the other terms are the mutual impedances describing the coupling effects between chips.
Combining equations (2.2) and (2.3), the complete model can be written in matrix-form as:

$$z_{th}P = \Delta T \quad (2.4)$$

where z_{th} is the $n \times n$ thermal impedances matrix, P is the $n \times 1$ vector of the input powers $P=[P_1, P_2, \ldots, P_n]^T$ and $\Delta T=[T_1-T_r, T_2-T_r, \ldots, T_n-T_r]^T$ is a $n \times 1$ vector of the differences between the temperature chip T_i and the reference temperature T_r.

2.3 Lumped parameter modeling

The thermal data extracted by the FE model are used to derive an equivalent RC network. This is possible thanks to the analogy between thermal and electrical quantities as reported in Table I.

TABLE I:
Analogy between thermal and electrical quantities.

Thermal power	Electrical current
Temperature difference	Voltage difference
Thermal capacity	Electrical capacity
Thermal resistance	Electrical resistance

The aforementioned analogy leads to a wide use of RC passive circuits topologies to reproduce the thermal behavior of a power device [43]. The typical passive topology used to estimate the junction temperature of a chip is the RC Foster network [42] shown in Figure 2.3a. The junction temperature estimation (and consequently the linearly related thermal impedance) is given from the voltage drop across the input port. Nevertheless, the use of RC Foster networks for the reproduction of the thermal impedances is not always suitable. In fact, we have found that this approach works well to reproduce the thermal self impedance behavior but is not able to fit properly the mutual impedance.

The reason of this is related to the delay characterizing thermal mutual impedances as underlined in Section 2.4. This delay increases when the distance between chips grows.

In [37], another strategy to address the reproduction of thermal mutual impedances behavior is based on the use of mathematical relations. The approach proposed in this paper deals with this problem in the framework of passive networks by defining adequate topologies for the two cases of self and mutual impedances. Specifically, the Foster type network of Figure 2.3a is used to reproduce the self impedances behavior, while thermal mutual impedances are modeled by means of the circuit topology of Figure 2.3b.

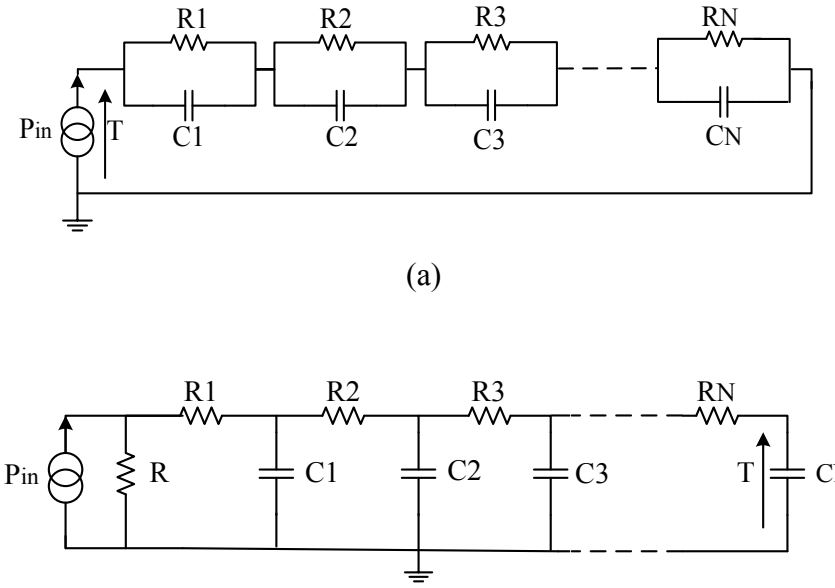

Figure 2.3: RC passive networks: a) Foster RC-network for thermal self impedance; b) RC-network for thermal mutual impedance.

By comparing the circuit of Figure 2.3a with the circuit of Figure 2.3b it is possible to point out that the temperature used to calculate the thermal impedances is evaluated at different network points. In fact, in the circuit of Figure 2.3b the output is evaluated as the voltage drop across C_N. In the case of mutual impedance the temperature of the device changes as the result of heating the device *j*, and heat transfer occurs through several layers (involving different thermal capacity-resistance terms).

This topology, as shown in Section 2.4, allows to fit properly the transient part of the mutual impedances.

The transfer function for the RC Foster type network (Figure 2.3a) is:

$$F(s) = \frac{T(s)}{P_{in}(s)} = \sum_{n=1}^{N} \frac{R_n}{1 + sR_nC_n} \qquad (2.5)$$

while the transfer function of the RC network used for the thermal mutual impedances reproduction (Figure 2.3b) is obtained by following the procedure described in [49],[50]. Specifically, let us define the transfer function $H_k(s)$ for each cell (RC group) composing the circuit of Figure 2.3b as

$$H_k(s) = \frac{Vout_k(s)}{Vin_k(s)} = \frac{1}{1 + sR_kC_k} \qquad k = 1, \dots, N \quad (2.6a)$$

while for the first cell made only of the resistor R, it holds:

$$H_0(s) = \frac{Vout_0(s)}{Pin(s)} = R \qquad (2.6b)$$

Let indicate with $G_{in,k}(s)$ and $G_{out,k}(s)$ the input and output electrical impedance of the *k*-th cell:

$$G_{in,k}(s) = R_k + \frac{1}{sC_k} \quad k = 1, \dots, N \quad (2.7)$$

$$G_{out,k}(s) = \frac{G_{out,k-1} + R_k}{sC_k \cdot \left(G_{out,k-1} + R_k + \frac{1}{sC_k}\right)} \quad k = 1, .., N \quad (2.8a)$$

$$G_{out,0}(s) = R \quad (2.8b)$$

Let us further introduce the quantities:

$$G_k(s) = \frac{G_{in,k+1}(s)}{G_{in,k+1}(s) + G_{out,k}(s)} \qquad k = 0, \dots, N-1 \quad (2.9)$$

$$H(s) = \prod_{k=0}^{N} H_k(s)$$
$$G(s) = \prod_{k=0}^{N-1} Z_k(s) \qquad (2.10)$$

Then, from equations (2.10) through equations (2.6)-(2.9) the transfer function of the RC circuit in Figure 2.3b is:

$$F(s) = \frac{T(s)}{P_{in}(s)} = H(s)G(s) \qquad (2.11)$$

The unit step response functions of circuits 3a and 3b describe the self thermal impedance and the mutual thermal impedance, respectively.

The form of these step response functions motivates the choice of the topology in Figure 2.3b. Typically, thermal mutual impedances show a quite slow transient due the horizontal heat propagation through the layers of the module. In mathematical terms this is expressed by the fact that the Taylor expansion around $t = 0$ of the thermal response $z(t)$, that is

$$z(t) = z(0) + \frac{z'(0)}{1} \cdot t + \frac{z''(0)}{2!} \cdot t^2 + \cdots \qquad (2.12)$$

needs to have small coefficients $z'(0)$, $z''(0)$, ... ($z(0)=0$ as it starts from zero initial conditions).

In particular, the network of Figure 2.3b allows to obtain a step response function having all coefficients $z'(0), \ldots, z^{n-1}(0)$ exactly equal to zero, thus facilitating to match the slow transient shown by FE results. In the following we relate the coefficients in the Taylor expansion of the step response function (2.12) with the coefficients of the transfer function of the networks of Figure 2.3a and 2.3b.

Let be $F(s)$ the transfer functions $\frac{T(s)}{P_{in}(s)}$ of the network in Figure 2.3a and 3b:

$$F(s) = \frac{b_1 s^{n-1} + b_2 s^{n-2} + \cdots + b_n}{s^n + a_1 s^{n-1} + \cdots + a_n} \qquad (2.13)$$

Let us indicate with $Z(s) = \frac{F(s)}{s}$ the unit step response of the two types of networks. Then, the initial value theorem can be used to estimate the coefficient $z'(0)$. In fact, it holds under the hypothesis of zero initial conditions $z(0) = 0$:

$$z'(0) = \lim_{t \to 0} z'(t) = \lim_{s \to +\infty} s^2 Z(s) = \lim_{s \to +\infty} s\, F(s) = b_1 \qquad (2.14)$$

We notice that for the network of Figure 2.3a, being $F(s)$ a positive real function, $b_1 \neq 0$. In fact, the circuit of Figure 2.3a is a relaxation system [58] with alternated finite zeros and poles and positive residues. Thus, the relative degree of this transfer function is always equal to one. This implies that in a neighborhood of the time origin the step response of the network will have a positive slope. On the contrary, for the network of Figure 2.3b we show that $b_1 = 0$, implying that the step response will start with a null slope. Furthermore, $b_i = 0,$ for $i = 1,..,n-1$, nullifying the corresponding contribution of the high-order Taylor terms to the growth of the network step response. In fact, when $b_1 = 0$, for network of Figure 2.3b, we can calculate $z''(0)$ as:

$$z''(0) = \lim_{t\to 0} z''(t) = \lim_{s\to +\infty} s^2 Z(s) = b_2 \qquad (2.15)$$

And with an analog procedure also the high order coefficients $\mathrm{z'''(0) = b_3, \dots, z^{n-1}(0) = b_{n-1}}$ are found to be zero for the network of Figure 2.3b. In fact, the Ladder network with the capacitors configuration as in Figure 2.3b is a low-pass filter with a transfer function having no finite zeros [59]. As an example we consider the identification of a thermal self impedance and a mutual one [31]. In particular we consider $z_{11}$and z_{21}. We have $\mathrm{Z_{11}(s) = \frac{F_{11}(s)}{s}}$ and $\mathrm{Z_{21}(s) = \frac{F_{21}(s)}{s}}$ with

$$F_{11}(s) = \frac{305.5018\,(s+7429)\,(s+428.1)\,(s+51.35)}{(s+1.907\cdot 10^4)\,(s+2997)\,(s+124.1)\,(s+23.61)}$$

$$F_{21}(s) = \frac{63303949.4893}{(s+2.575\cdot 10^4)(s+101.9)(s+55.65)(s+14.75)}$$

where the transfer functions have been obtained with the values specified in Table I. It is evident that $\mathrm{F_{21}}$ has no finite zeros and is characterized by a relative degree four while $\mathrm{F_{11}}$, having three zeros, is characterized by a relative degree one.

The unit step response of $F_{11}(s)$ and $F_{21}(s)$ is shown in Figure 2.4. In contrast to the thermal self impedance behavior, the mutual impedances are affected by a delay related to the distance between chips. Moreover, as underlined in the case study proposed in [31], it is possible to observe that the higher is the distance between chips, the higher will be the delay and the smaller will be the thermal coupling described by the thermal mutual impedances.

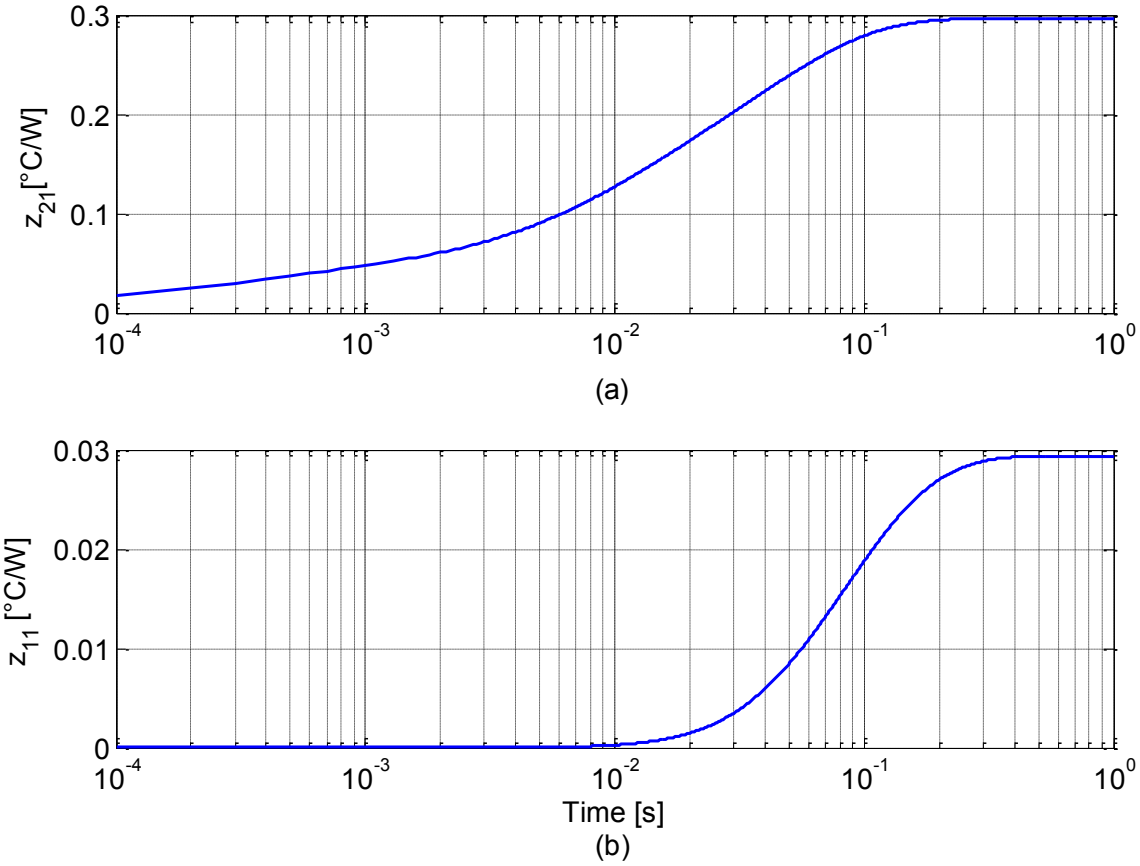

Figure 2.4: a) Unit step response of $F_{11}(s)$; b)Unit step response of $F_{21}(s)$;

TABLE I:
RC NETWORK PARAMETERS

	z_{11} [°C/W]	z_{21} [°C/W]	z_{31} [°C/W]	z_{41} [°C/W]
R [Ω]	-	0.0294	0.0107	0.0024
R_1 *[Ω]*	0.0114	0.0042	0.0015	0.0104
C_1 *[F]*	0.0046	0.4816	2.3097	3.3168
R_2 *[Ω]*	0.0727	0.3024	0.0040	0.2610
C_2 *[F]*	0.1108	0.0478	1.8722	0.1656
R_3 *[Ω]*	0.0249	1.1730	0.0639	4.3448
C_3 *[F]*	0.0134	0.0002	0.4014	0.0087
R_4 *[Ω]*	0.1888	0.2338	0.9098	54.6838
C_4 *[F]*	0.2243	0.0362	0.0374	0.0008

To identify the model parameters *R* and *C* of equations (2.5) and (2.11) the Nelder-Mead simplex optimization method [51], [52] is used. The parameters identification was performed by comparison of the thermal impedance provided by the FE simulations, $z_{FE}(t)$, with the unit step response, $z_{RC}(t)$, of the systems described by equations (2.5) and (2.11).

More specifically, the objective function (J_{err}) to be minimized takes into account the error between the two impedances and their time derivatives:

$$J_{err} = \sqrt{\frac{1}{\tau}\int_0^{\tau}[\,z_{RC}(t) - z_{FE}(t)]^2 dt} + \frac{k}{2}\sqrt{\frac{1}{\tau}\int_0^{\tau}[\,z'_{RC}(t) - z'_{FE}(t)]^2 dt} \qquad (2.16)$$

in which the first term is the Euclidean norm of the error between z_{RC} and z_{FE} while the second term is the Euclidean norm of their time derivatives and τ is the observation time. In our work we fixed τ =10s. Equation (2.16) is a multi objective function that takes into account the error in both the impedances and their time derivatives estimates (with $k = 1\ s^{-1}$). It is worth noticing that the first term of equation (2.16) is not able to ensure a good fit of the transient part of the impedance, characterized by a relevant slope. For such a reason the second term, based on the impedance time derivatives, has been introduced. The proposed approach can be used to properly reproduce all self and mutual impedances and then to describe the whole module thermal behavior. Thanks to the system linearity, the superposition principle can be applied and the thermal impedances extracted from circuits can be added according to equation (2.4). This means that by combining all derived RC circuits, as shown in Figure 2.5, it is possible to simulate in a fast and efficient way the module thermal behavior by means of a generic circuit simulator. Eventually, data acquired by using an experimental setup are used to validate the approach against real data.

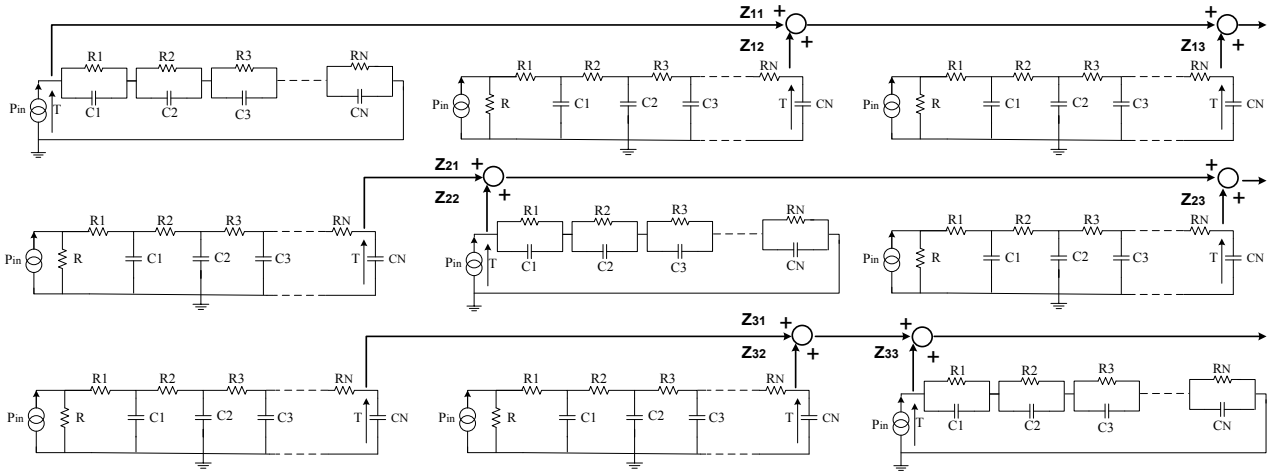

Figure 2.5: RC circuits describing the thermal behavior of three different chips

The approach proposed in this thesis is general as it can be used to extract the thermal networks either from FE models or experimental data of thermal impedances. Furthermore, the number of variables in the model is reduced by starting from physical considerations enabling the identification of the points to be used to build the model, that is, for instance, the temperatures of selected locations of the module (IGBTs and diodes). Finally, the order of the obtained model is typically low. The aforementioned methodology has been applied successfully for a case of study proposed in [31].

3

Identification of nonlinear oscillations in high power systems by using neural networks

In this Chapter a brief presentation of the use of neural networks to identify nonlinear oscillations in JET plasmas in [20] and [60] is introduced. Then, the methodology used to predict JET instabilities is discussed in detail.

3.1 Introduction on Artificial Neural Networks (ANN)

Artificial neural networks (ANN) are mathematical models, inspired by the structure of biological neural networks, made up of elementary units called neurons which are able to perform simple computations [61], [62]. They are used to solve classification and nonlinear functions approximation problems. One of the neural network features is to be inspired to the structure of the human brain, taking advantage from the main feature, the ability to learn from experience. Neural networks require a training phase using examples to acquire the experience necessary to provide the correct output in the face of new inputs.

Advantages:

- A neural network can perform tasks that a linear program cannot.
- When an element of the neural network fails, it can continue without major problems by their parallel nature.
- A neural network learns and does not need to be reprogrammed.
- It can be implemented in any application.
- It can be implemented easily.

Disadvantages:

- The neural network needs training to operate.
- The architecture of a neural network is different from the architecture of microprocessors therefore needs to be emulated.

- Requires high processing time for large neural networks.

Artificial neural networks (ANNs) are among the most attractive signal processing technologies in the engineer's toolbox [61]. The field is highly interdisciplinary, but our approach will restrict the view to the engineering perspective. In engineering we can define an artificial neural network as an adaptive, most often nonlinear system, that learns to perform a function, an input/output map, from data. Adaptive means that the system parameters are changed during operation, normally called the training phase. After the training phase the ANN parameters are fixed and the system is deployed to solve the problem at hand in testing phase. The input/output data are fundamental in neural network technology, because they convey the necessary information to discover the optimal operating point. The nonlinear nature of the neural network processing elements provides the system with lots of flexibility to achieve practically any desired input/output map, so some ANNs are universal approximators [64], [65].

3.2 Mathematical representation of a single neuron

Let us consider an ANN as a computational system densely connected that is able to store knowledge by means of experiments. The acquired knowledge is stored using the values of some parameters, called weights, which connect the computational units, called neurons, whose values are fixed during the training phase. Each neuron is an entity that has multiple inputs and one output, so is a MISO (Multi input single output) system [62]. It receives inputs from neighboring neurons, processes them and sends the output to other neurons weighing it appropriately. The currently most widely used neuron model is shown in Figure 3.1 where x_i is the *i*-th input, w_i is the weight of the *i*-th input and $f(W^tX + \text{bias})$ is a function, usually non linear, called activation function. The neuron has a bias which is added to the inputs weighted sum with a unit weight. The sum $n = W^tX + \text{bias}$ is called net input. The output of the neuron is the value of the activation function at the net input.

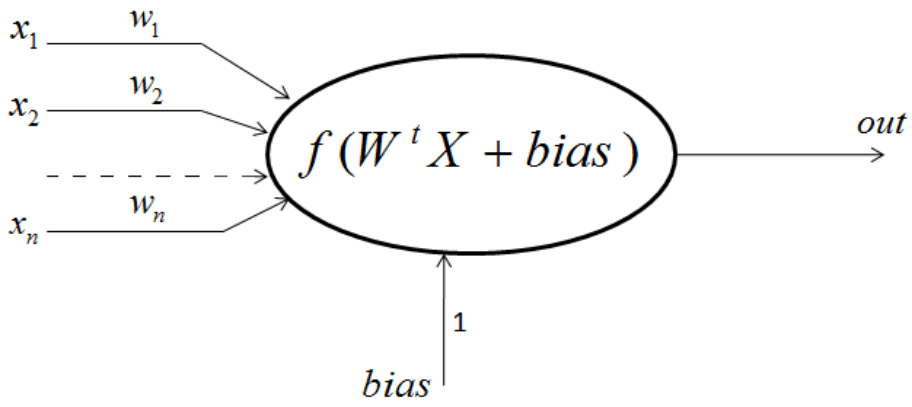

Figure 3.1: Artificial neuron.

The output of the neuron is then given by the formula:

$$\text{out} = \text{f}\left(\sum_{\text{i=1}}^{\text{n}} \text{w}_\text{i}\text{x}_\text{i} + \text{bias}\right) = \text{f(n)} \qquad (3.1)$$

Each neuron can use different activation functions to generate its own output. Let us consider, as shown in figures Figure 3.2 that a is the neuron's output while n is the net input.

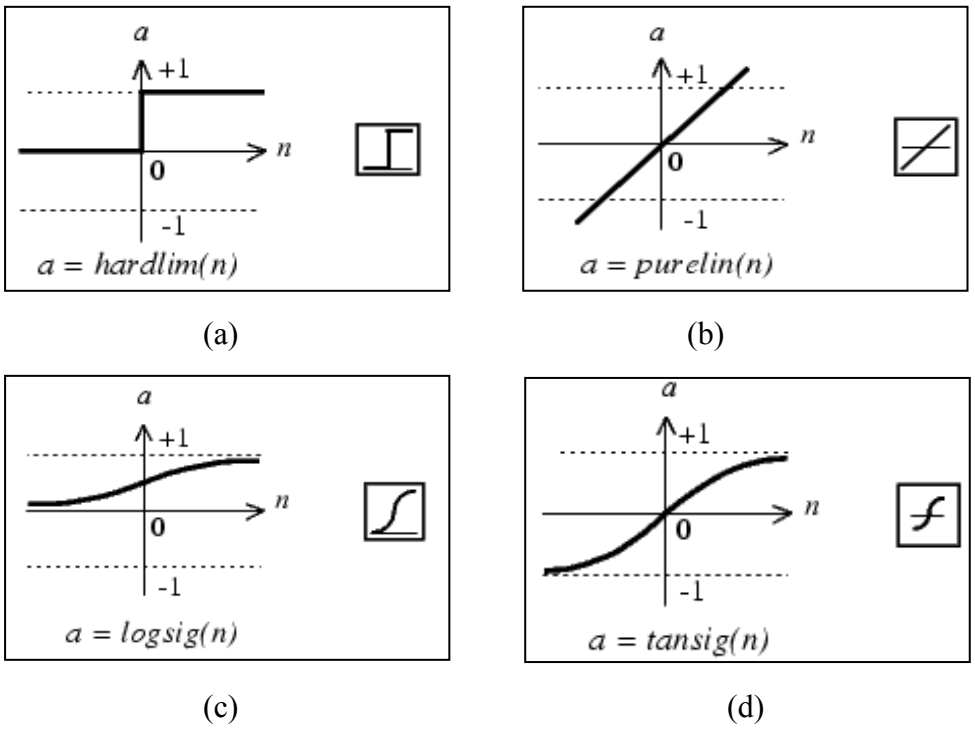

Figure 3.2: Activation functions of an ANN: (a) hard limit, (b) linear, (c) sigmoid, (d) hyperbolic tangent.

3.3 Description of layers

As shown on Figure 3.3, a layer [61]-[65] consists of S neurons working in parallel. Each unit performs a relatively simple job: it receives input from neighbors or external sources and uses this to compute an output signal which is propagated to other units. All neurons take their inputs from the same input vector $p = [p_1, p_2, \dots, p_R]$ (containing R inputs). If the layers have S neurons, then the layer output will be a S sized vector. As a result, the weight matrix W is an S*x*R sized matrix, the bias vector b and the output vector a are vectors containing S elements.

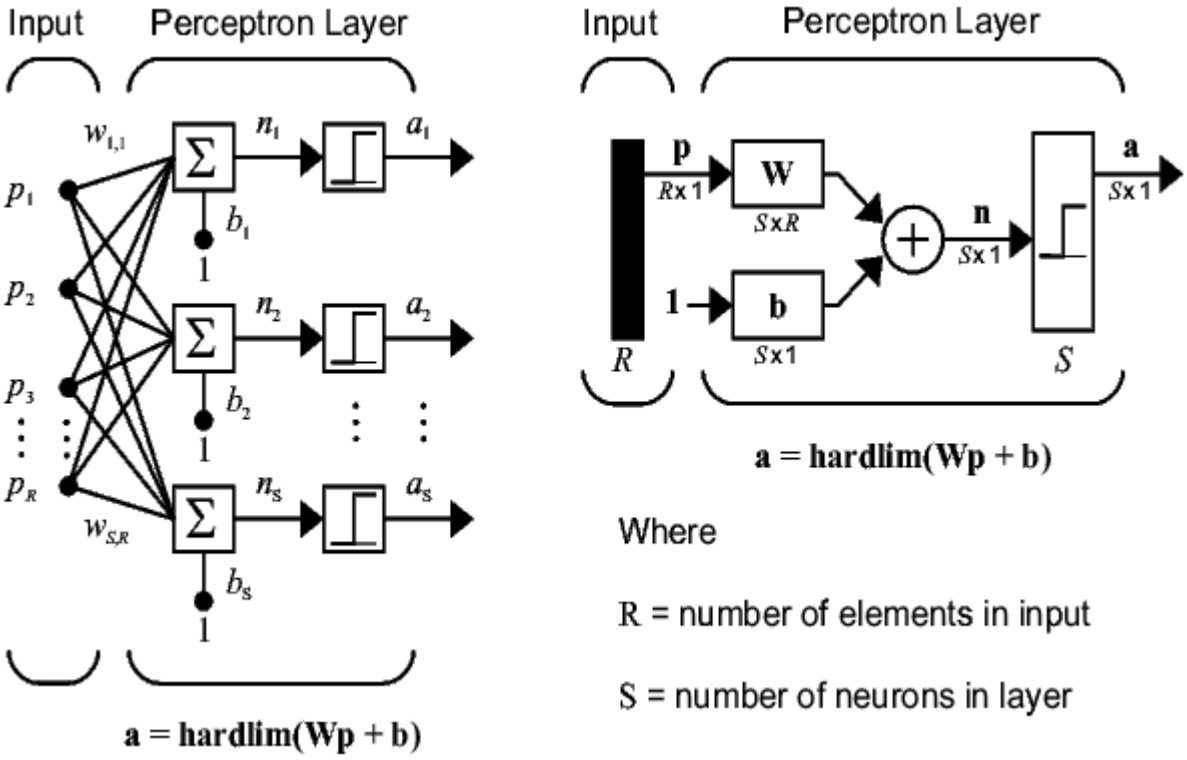

Figure 3.3: A hard limit neural layer. Left: detailed architecture of a neural layer. Right: compressed notation of a neural layer.

Each neuron of the same layer has the same activation function f. We can write the layer output vector, $a = [a_1, a_2, \dots, a_s]$, as a product of matrices:

$$Y = f(Wp + b) \qquad (3.2)$$

where

$$W = \begin{bmatrix} w_{11} & \dots & w_{1R} \\ \vdots & \ddots & \vdots \\ w_{S1} & \dots & w_{SR} \end{bmatrix}, a = \begin{bmatrix} a_1 \\ \vdots \\ a_S \end{bmatrix}, b = \begin{bmatrix} b_1 \\ \vdots \\ b_S \end{bmatrix}, p = \begin{bmatrix} p_1 \\ \vdots \\ p_R \end{bmatrix},$$

in fact the output of the *j*-th neuron is calculated as:

$$a_j = \sum_{i=1}^{R} w_{ij} \cdot p_i + b_j \quad (3.3)$$

3.4 Training

Before using a neural network, weights and biases have to be adjusted [61]. Training is a process, to adjust the network coefficients, that requires a set of examples of proper network behavior. The training process is performed by means of learning algorithms which depend on the kind of network used. There are several learning approaches each corresponding to a particular abstract learning task. These are supervised learning and unsupervised learning.

The learning algorithms are called supervised when, during the training, we apply to the network an input-output dataset. The objective is to determine an adaptive algorithm or rule which adjusts the parameters of the network based on a given set of input-output pairs. If the weights of the network are considered as elements of a parameter vector ϑ, the learning process involves the determination of the vector $\bar{\vartheta}$ which optimizes a performance function J based on the output error. The simplest method used for this purpose is back propagation [65] in which the gradient of the performance function with respect to ϑ is computed as $\nabla_\vartheta J$ and ϑ is adjusted along the negative gradient as

$$\vartheta = \vartheta_{nom} - \eta \nabla_\vartheta J|_{\vartheta=\vartheta_{nom}} \quad (3.4)$$

where η, the step size, is a suitably chosen constant and ϑ_{nom} denotes the nominal value of ϑ at which the gradient is computed.

The weights and biases of the network are then iteratively adjusted to minimize performance function that is typically the mean square error between the network outputs and the target outputs. When the training begins, initial weights and biases are initialised randomly. This haphazard initial conditions permit to avoid falling always in the same local minima of a function. The training method is based on gradient descent therefore, the network can fall in an error local minimum if it always starts from the same initial weights.

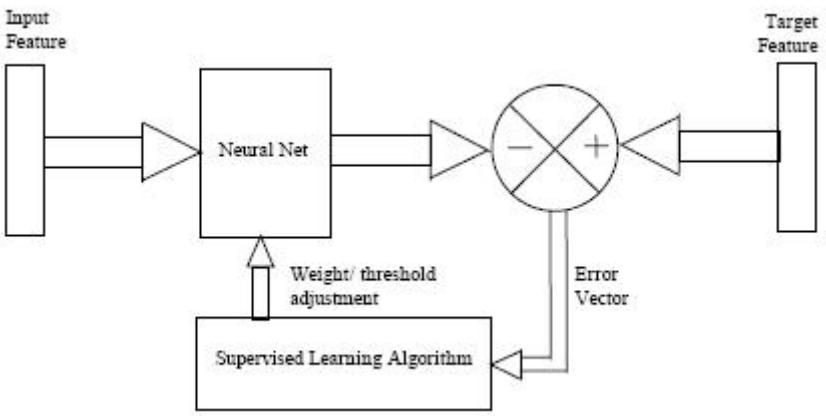

Figure 3.4**:** Example of a neural network training by means of a supervised learning algorithm.

The learning algorithms are called "unsupervised" when we feed the network without the correct outputs. These algorithms are used to classify inputs in different classes identified by a different output value of the network.

Once training is complete we need to test the network to verify that it works correctly. In this phase we apply a different dataset than that used in training phase and the weights are maintained fixed. It is necessary to verify that error is sufficiently low with these new sets of data. If the error is too high, it's both possible that network topology is wrong or that the training patterns aren't representative of the underlying problem.

3.5 Neural network topologies

In general, a neural network consists of [63], [65]:

1) A layer of input neurons, which only has the task of transferring input signals from outside of the neural network to the next layer, weighing them appropriately;

2) One of more intermediate layers, also called hidden layers, whose input and output signals remain within the neural network. The hidden layer is characterized by neurons with nonlinear activation function. It allows the network to learn nonlinear and linear relationships between input and output vectors.

3) An output layer of neurons that produces the outputs of the network.

This section focuses on the pattern of connections between the units and the propagation of data. As for this pattern of connections, the main distinction we can make is between:

- Feed-forward neural networks where the data flow from input to output units is strictly feed-forward. The data processing can extend over multiple (layers of) units, but no feedback connections are present, that is, there are no connections extending from outputs of units to inputs of units in the same layer or previous layers.
- Recurrent neural networks (RNNs) that do contain feedback connections.

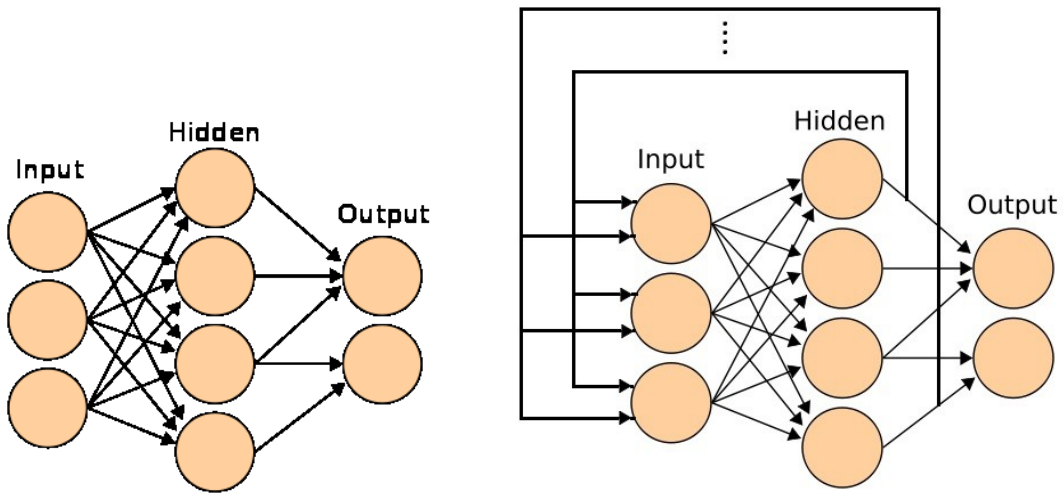

Figure 3.5: Neural networks topologies. On the left: feed-forward neural network. On the right: recurrent neural network.

RNNs work cyclically :

- its outputs are calculated from the inputs;
- outputs are passed into the input of the RNN.

These two steps are clearly separated and could be executed in the same time. RNNs have interesting dynamics property because they calculate their output taking into account the past. Feed forward neural networks are less powerful than RNNs because they can model only static functions.

In mathematics, the universal approximation theorem [66] states that the standard multilayer feed-forward network with a single hidden layer that contains finite number of hidden neurons, and with arbitrary activation function are universal approximators on a compact subset of R_n.

The theorem was proved by George Cybenko in 1989 for a sigmoid activation function, thus it is also called the Cybenko theorem.

Theorem 1: Any continuous multivariate function can be approximated with an arbitrary precision by a one hidden layer feed forward neural network (Cybenko, 1989). The first layer should have a sigmoid type transfer function. Its number of neurons depends on the quality of approximation, the more there are, the best it is. The second layer should be a pure linear transfer function.

Theorem 2: Any multivariate function can be approximated with an arbitrary precision by a two hidden layer feed forward neural network. The first and second layer should have a sigmoid type transfer function. The output layer should be pure linear transfer function.

3.6 Identification of JET instabilities using neural networks

As introduced in chapter 1 the identification of plasma instabilities occurring during experimental pulses is of particular relevance for avoiding dangerous events in high performance discharges. In order to predict the onset of plasma instabilities, an identification method, based on the use of ANNs, has been applied in [20] and [60]. The potential of the networks to identify the dynamics of ELMs and sawtooth instabilities has been first validated using synthetic data obtained through a suitable mathematical model. The networks have then been applied to experimental measurement from JET pulses. An appropriate selection of the network topologies allows identifying quite well the time evolution of the edge temperature and of magnetic fields, considered the best indicators of the ELMs. A quite limited number of periodic oscillations are used to train the networks, which then manage to follow quite well the dynamics of the instabilities. Furthermore, a careful analysis of the various terms appearing in the rule identified by the ANNs gives clear indications about the nature of these instabilities and their dynamical behavior.

JET plasmas with evident macroscopic implications, such as ELMs, sawteeth and Neoclassical Tering Modes, are subject of active investigation. Among the difficulties in understanding the dynamics of these instabilities is the fact that the data analysis is often demanding and requires significant efforts. Automatic data analysis tools to identify the main aspects of the instabilities, from the signature they leave on the measurements, would therefore be quite beneficial. In the last few years, quite significant experience has been gathered in using new machine learning tools, which have a lot of potential and can be quite effective in identifying even complex systems. In particular the use of Artificial Neural Networks (ANN) are very powerful in identifying even quite complex dynamic behaviour, as shown for the case of coupled pendula in [67], for the identification of Topping process also in the case of small datasets [68], or for the analysis of nonlinear dynamics in a sulfur recover unit [69]. Among the possible configurations, a RNN approach has been adopted. The layout of RNNs can take many different forms but the ones, whose results are presented in this chapter, are the input-output type, which means that there is a basic feedback loop from the outputs to the input of the entire network. In Section 3.6.1 the main lines of the identification approach are discussed, in Section 3.6.3 the results for type I and type III ELMs and the core considerations on the proposed approach are discussed.

3.6.1 The identification approach

The general topology of the network used to identify the time trend of the edge temperature and of magnetic fields corresponds to the following generic ansats:

$$\begin{cases} T(n) = f_1[T(n-2)] + f_2[T(n-1)] + h_1[B(n-3)] + f_3[B(n-2)] + \\ \quad + f_4[B(n-1)] + f_5[B(n)] \\ B(n) = l_2[(T(n-3)] + g_1[T(n-2)] + g_2[T(n-1)] + l_1[(T(n)] + \\ \quad + g_3[B(n-3)] + \ + g_4[B(n-2)] + g_5[B(n-1)] \end{cases} \tag{3.5}$$

The topology of the network implementing ansatz (3.5) is shown in Figure 3.6. The squares correspond to nonlinear neurons, whereas the diamonds are linears ones. The activation function chosen for the nonlinear neurons is the sigmoidal functions (i.e. hyperbolic tangents).

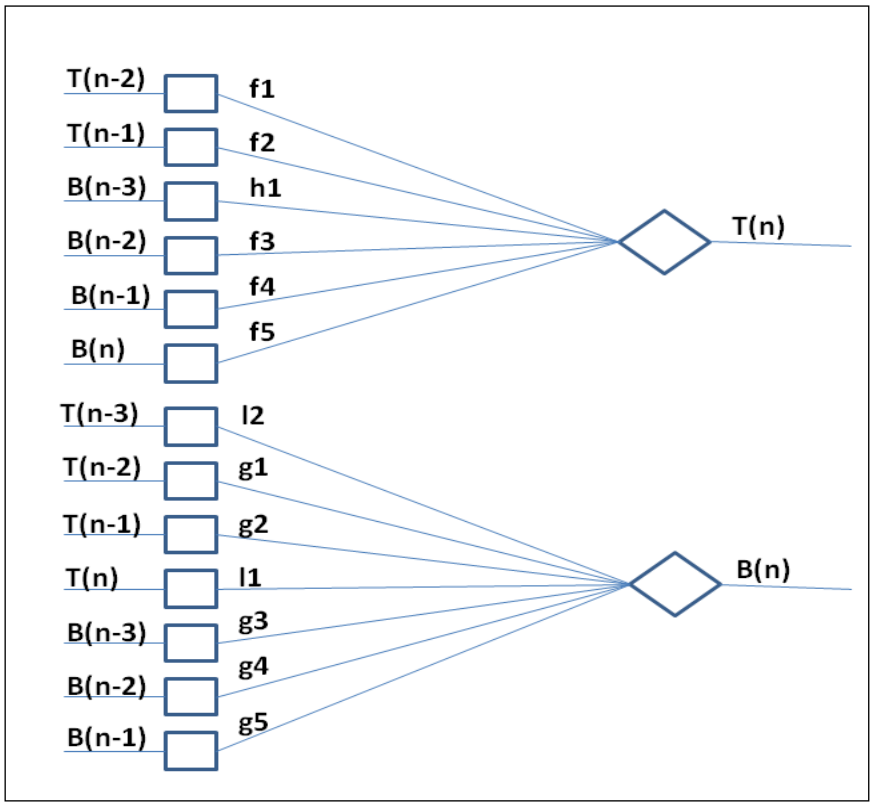

Figure 3.6: Topology of the network corresponding to the general "ansatz" of relation (3.5).

The training process consists first of the identification of a certain number of instability cycles with the one step ahead approach. The network is trained to estimate the signals at the next time step. In this sense, the network is trained as a feed-forward neural network. To prove the quality of the identification, the network is then applied in recurrent configuration by short circuiting the outputs to the inputs. This can be tested not only on the signals used for the training but also to subsequent

time intervals, considering that the parameters of the dynamic system are stationary. To assess the potential of the approach, the network has been trained and tested with synthetic signals obtained by using the model (1.2) reproducing the dynamics related to ELMs instability [21]. The shape of these synthetic signals has been chosen such that they are representative of experimental cases and also quite challenging because they present abrupt variations. In the same Figure 3.7 the outputs of the network and the original signals are both reported to show the quality of identification.

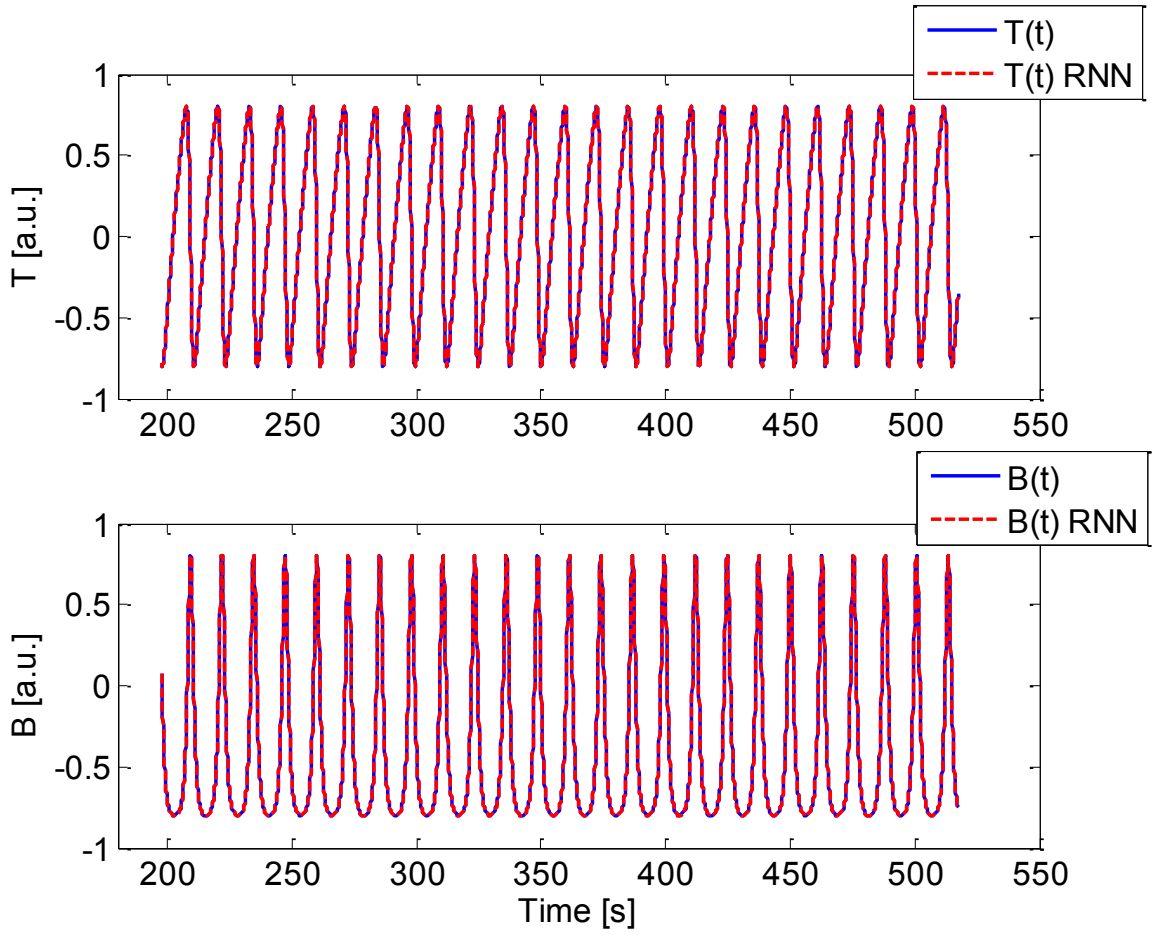

Figure 3.7: Continuous lines (blue): Synthetic signals used for the training; dashed lines (red): outputs of the ANN. The functions of relation (3.5) used to identify the signals are: f_1,f_2,f_3,f_4,g_1,g_2,g_3,g_4.

These outputs have been obtained with both outputs fed back to the inputs, so with both branches of the network in recurrent configuration, starting from suitable initial conditions.

3.6.2 Examples of ELM identification

As a relevant experimental example, the previously described approach has been applied to the identification of ELMs on JET. Since various types of ELMs have been experimentally and theoretically investigated, the long term goal of this type of work could be the automatic discrimination of the various types of ELMs. In this perspective, the first step consists of proving the capability of RNNs to identify the experimental signals, which present clear signatures of ELMs. After a careful analysis of the available signals, it has been decided to start by trying to identify the perturbations caused by the ELMs on the edge temperature, as measured by the Electron Cyclotron Emission Diagnostic (ECE), and on the magnetic field, as measured with the pick up coils. The former diagnostic system, ECE, is able to obtain time evolution of electron temperature with high temporal (~microsec) and spatial (~1cm) resolutions. Pickup coils are used to measure the component of the local magnetic field perpendicular to the plane of the coil. There are several pickup coils subsystems at JET placed in different positions [15]. In Figure 3.8 the pickup coil used in this study is shown.

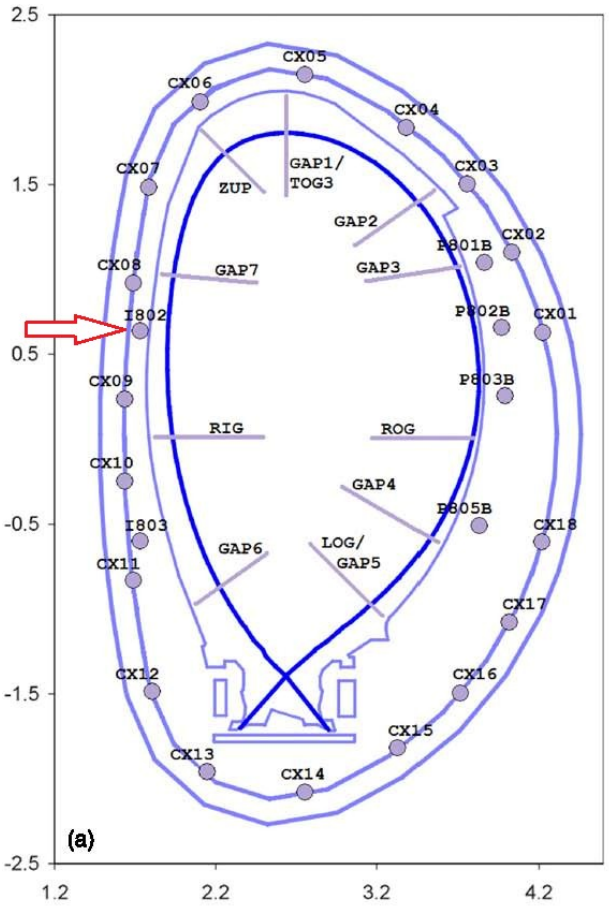

Figure 3.8: Position of the pickup coils around the first wall. The red arrows indicates the coil I802 used in this work.

Examples of the time evolution of these signals for type I and type III ELMs are reported in Figure 3.9 andFigure **3.10**.

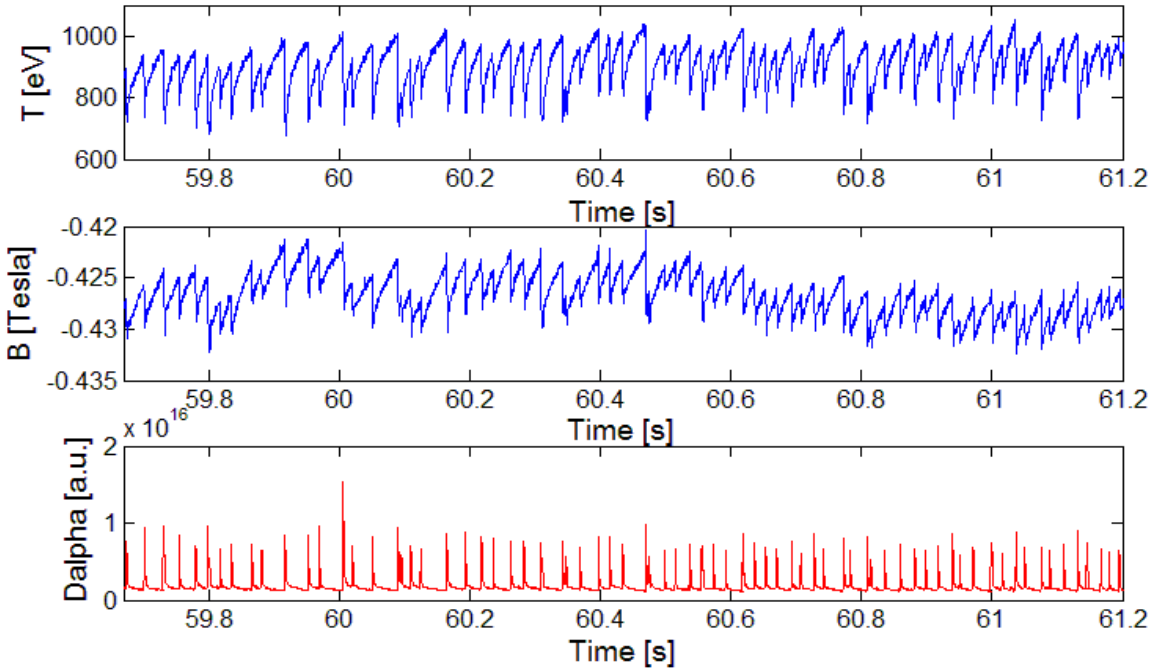

Figure 3.9: Time evolution of the signals for a type I ELM. Top: electron temperature at the radius measured with the ECE; middle: magnetic field measured with a fast coil; bottom: a Dα signal in the outer divertor.

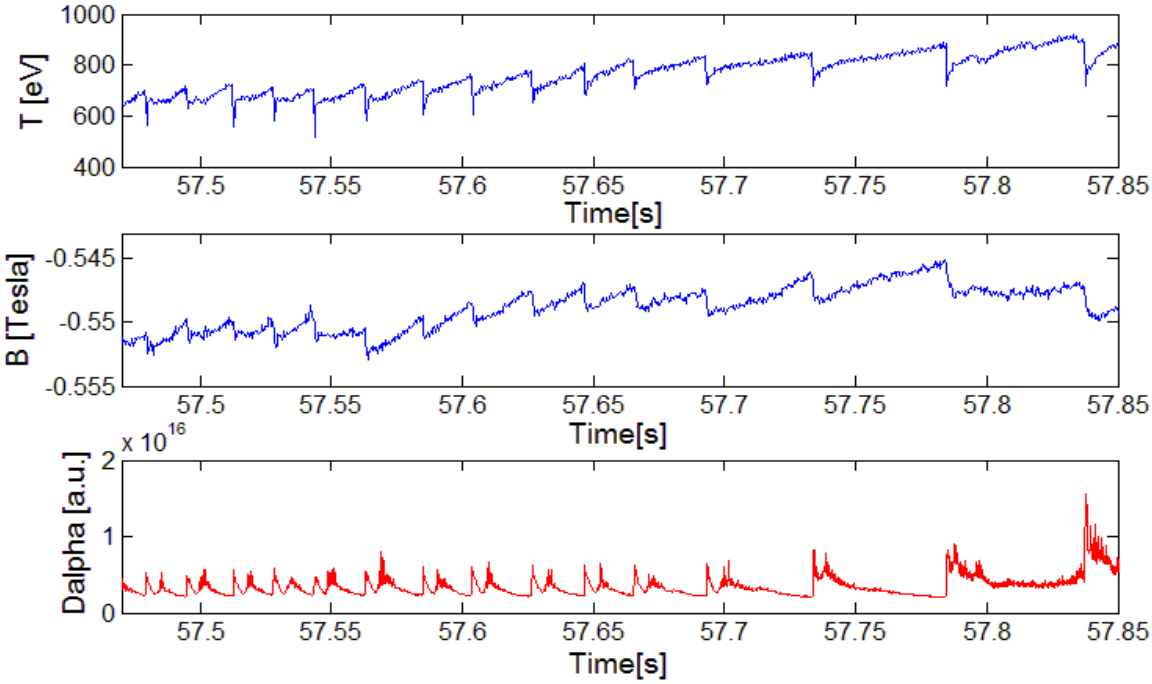

Figure 3.10: Time evolution of the signals for a type III ELM. Top: electron temperature at the radius measured with the ECE; middle: magnetic field measured with a fast coil; bottom: a Dα signal in the outer divertor.

The D_α signal is unfortunately too affected by the atomic physics at the edge and is therefore not a good descriptor of the ELM instabilities for the purposes of identification, which are the subject of this work. Given the quality of the signals and the fact that the discharges are not strictly stationary, some form of signal preprocessing is necessary. Filtering, to eliminate the highest frequency components of the noise, and detrending, to eliminate the slow drifts, are the first steps. Specifically, both signals T and B show abrupt variations, which correspond to high frequencies components. As a result, quick signals variations appear to be an essential part of the dynamics and cannot be filtered out. The main problem is to discriminate between the signals high frequency harmonics and noise. To detect the discontinuities, features of both signals, the first derivative of the signals using finite differences has been calculated :

$$\frac{dy}{dt}(n) \sim \frac{y(n+1) - y(n)}{h} \quad (3.6)$$

Noise induces also high derivatives and could be wrongly considered as a discontinuity. The only characteristic to distinguish high derivatives due to the dynamics of the signal from the ones caused by noise is the amplitude of the signal variations. Whereas the noise amplitude is very low, the discontinuity amplitude is higher. We can use this discrimination to separate noise from discontinuities.

We can therefore assume that we have a signal discontinuity when:

$$|y'(n)| > \mu * y'_{max} \quad (3.7)$$

where $y'_{max} = \max\left(\frac{dy}{dt}\right)$.

According to formula (3.7), we can choose a coefficient μ, which permits to discriminate parts of the curve with a high slope. After data filtering, detrending has been performed using an opportune low pass filter that exponentially cuts off the Fourier transform of signals above a certain frequency f_1:

$$Y(f) = \begin{cases} Y & f < f1 \\ Ye^{\left(-\frac{f-f1}{f2}\right)} & f > f1 \end{cases} \quad (3.8)$$

The filter parameters f_1 and f_2 are properly chosen in order to filter the flat noise component of the signal. An example of detrending is shown in Figure 3.11.

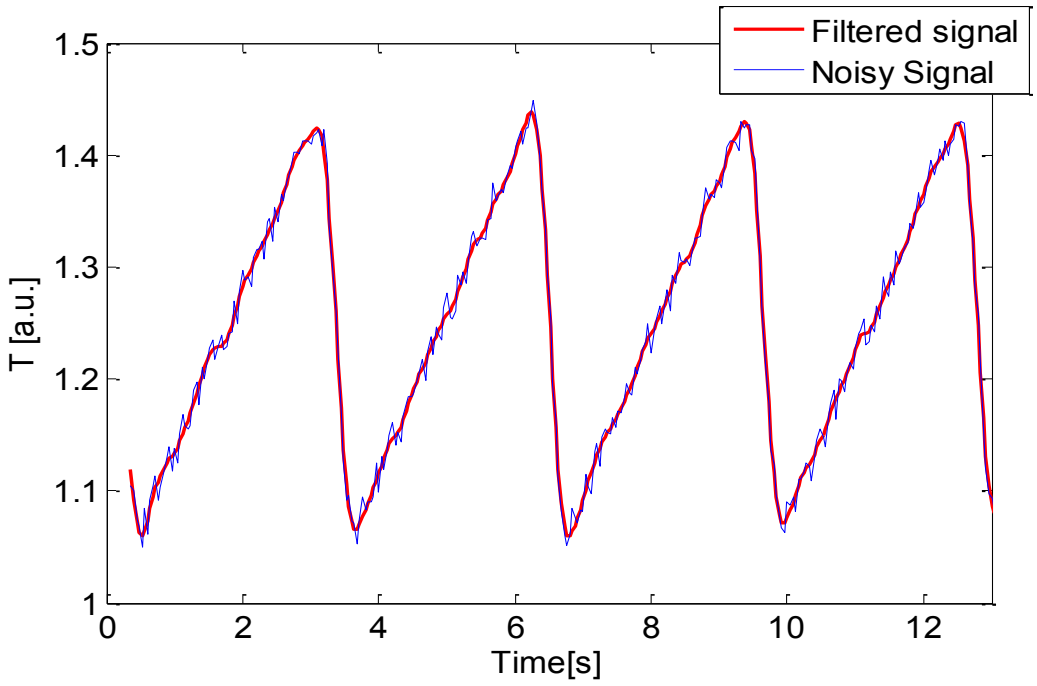

(a)

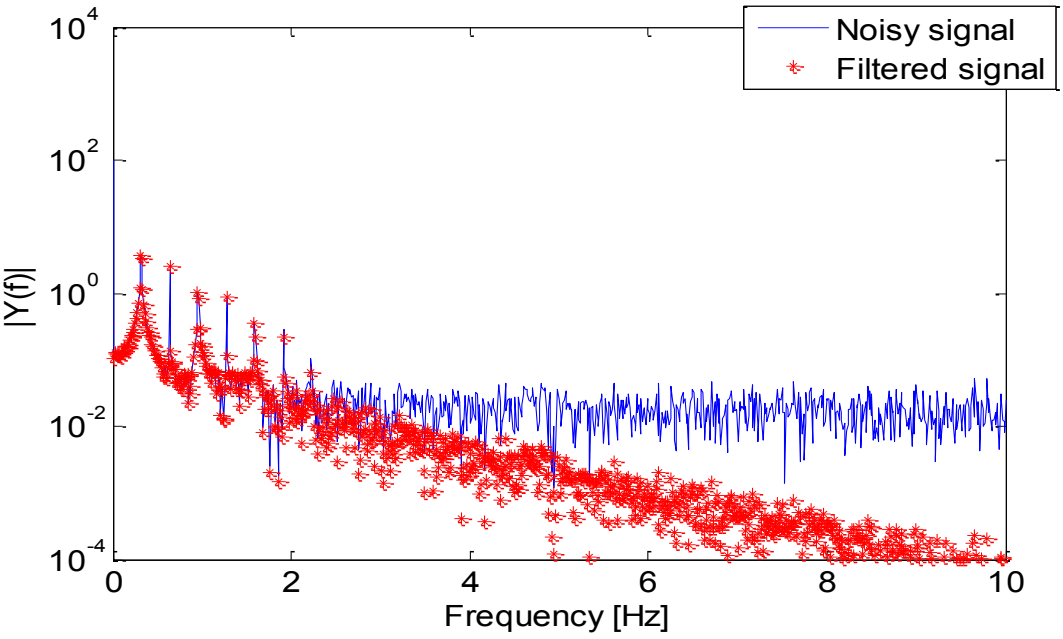

(b)

Figure 3.11: Detrending of signals: a) T signal versus time with noise (blue) and T filtered (red); b) Frequency spectrum of T with noise (blue) and filtered (red). $f_1=f_2=5$Hz.

The normalization of the signals is performed next to give to the RNNs inputs in the interval [-0.8,0.8] as required for the optimal use of the tanh activation functions to avoid saturation.

After identifying the signals with the network corresponding to the full topology, the weights of the various terms in Eq. (3.5) have been analysed. The smallest ones have been then eliminated up to the point when the performance of the networks degrades. This method allows converging on networks topologies with the minimum number of elements in the ansatz capable of learning the dynamics of the signals. For the ELM I case of Figure 3.9, the process converges on the following equations for the network:

$$\begin{cases} T(n) = f_1[T(n-2)] + f_2[T(n-1)] + f_4[B(n-1)] + f_5[B(n)] \\ B(n) = g_2[T(n-1)] + g_5[B(n-1)] \end{cases} \quad (3.9)$$

The test signals overlapped with the network outputs are shown in Figure 3.12.

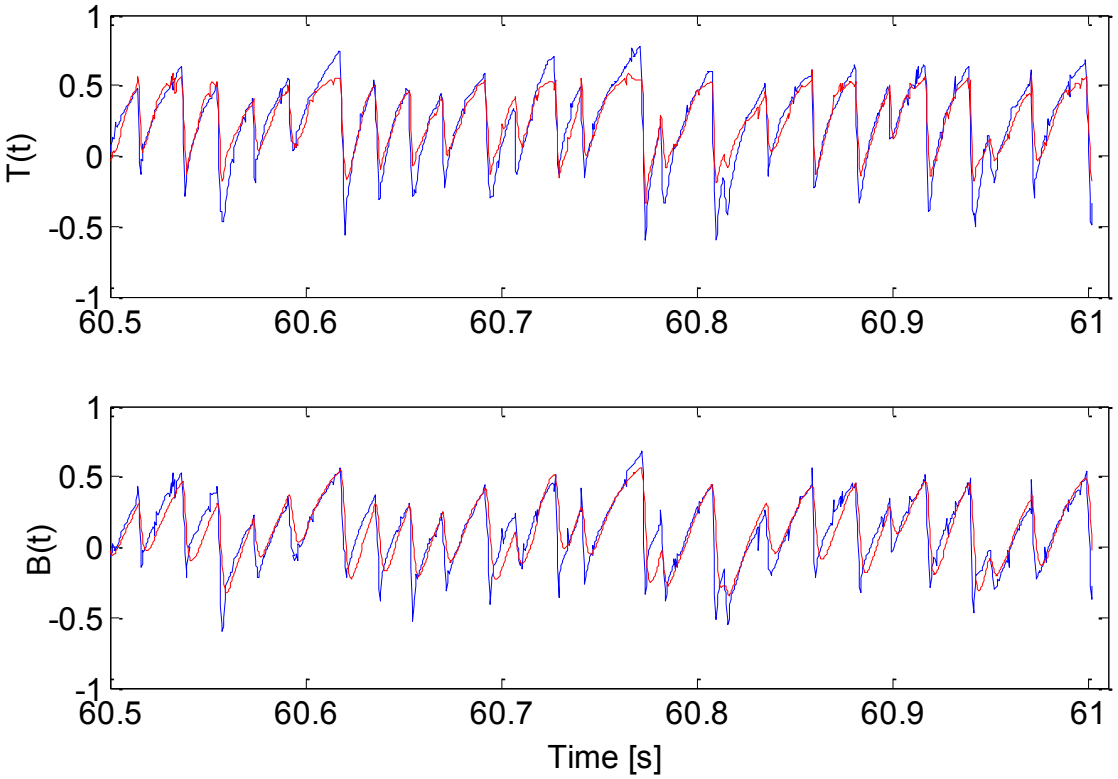

Figure 3.12: Top: test signal T (blue) and network output signal T (red) in recurrent configuration on T; bottom: test signal B (blue) and network output signal B (red) in recurrent configuration on B.

At this point the f and g functions can be extracted by analyzing the output of the corresponding non linear neuron. Specifically, according to the definition of neuron we can apply the following formula:

$$f(y) = LW_j \tanh(IW_j y + b_j) \quad (3.10)$$

where IW_j, LW_j and b_j are the input, output and bias weights of the non linear neuron *j*. For equations (3.9) the functions f and g are shown in Figure 3.13.

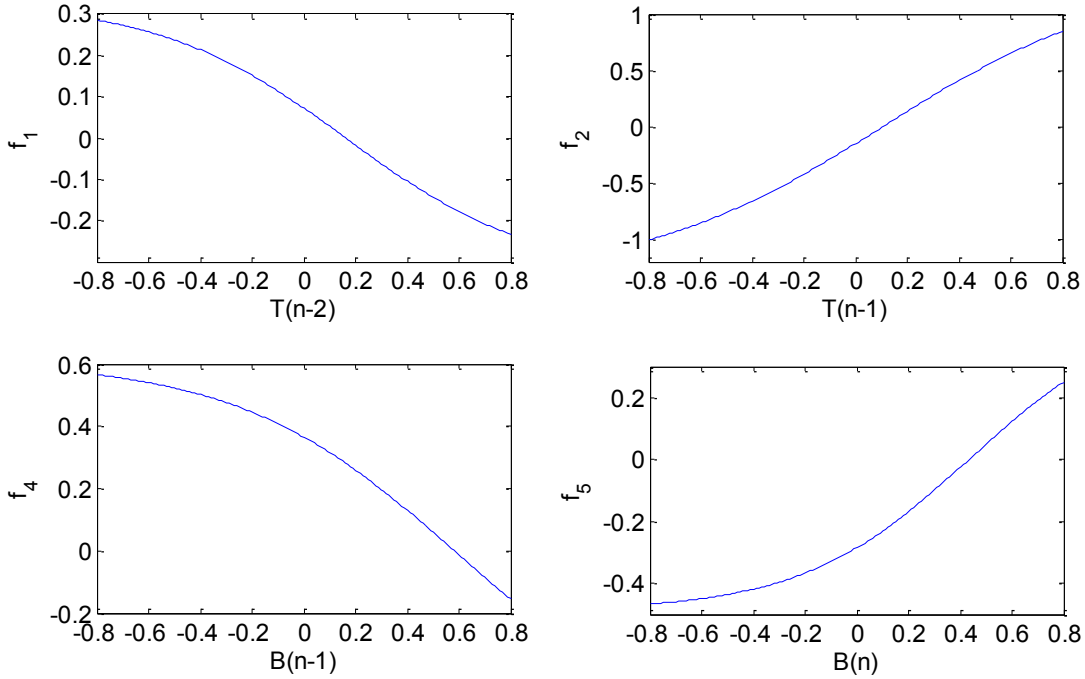

(a)

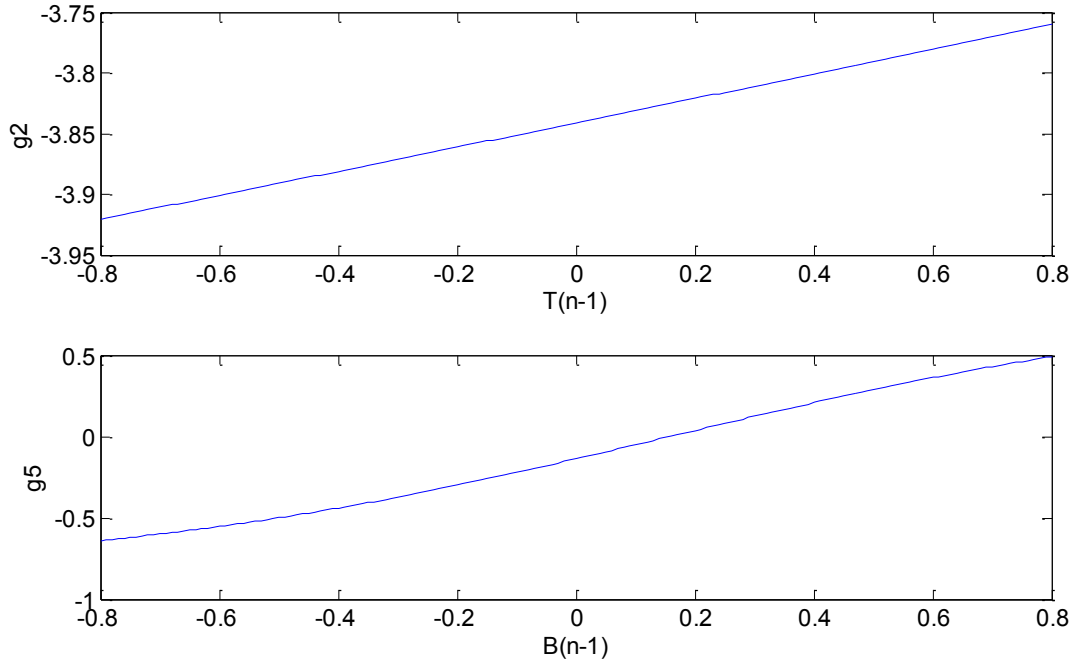

(b)

Figure 3.13: Nonlinear functions for equations (3.9): a) f_1, f_2, f_3, f_4 ; b) g_2, g_5

For the case of the type ELMs of Figure 3.10 , the final ansatz, after the elimination of the non relevant elements in Eq. (3.5) is:

$$\begin{cases} T(n) = f_3[B(n-2)] + f_5[B(n)] \\ B(n) = g_2[T(n-1)] + g_3[B(n-3)] + g_5[B(n-1)] \end{cases} \quad (3.11)$$

Test signals and network outputs are compared in Figure 3.14.

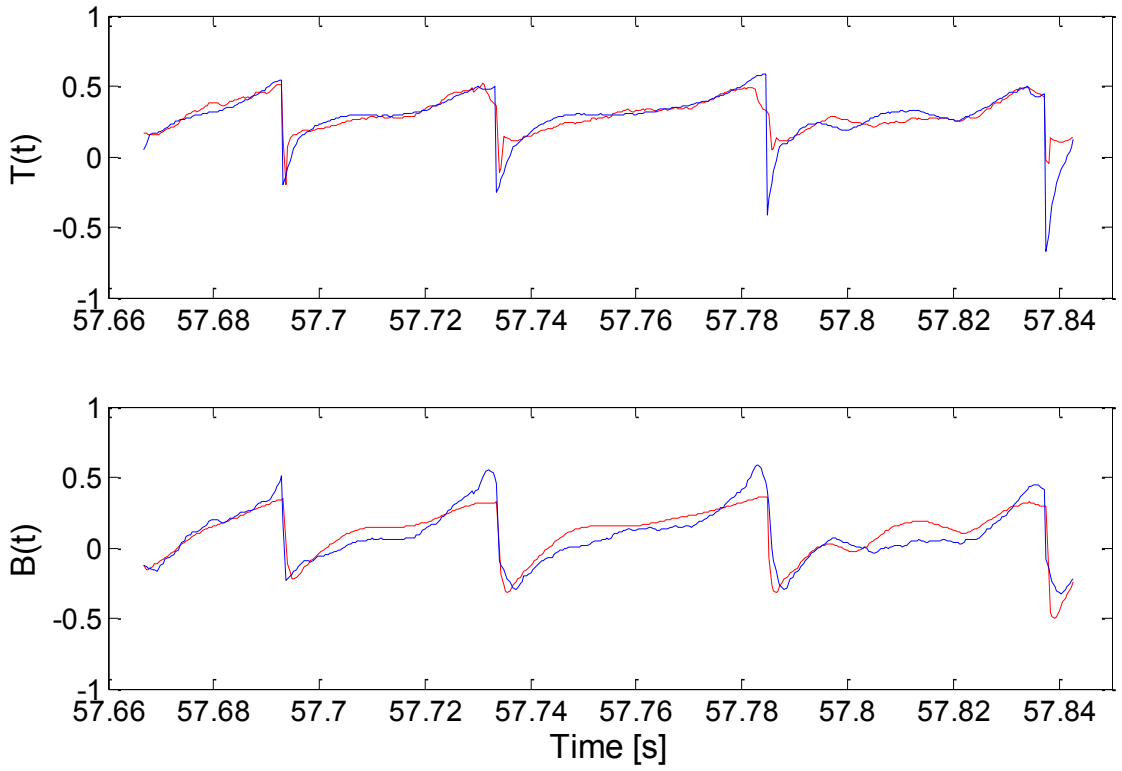

Figure 3.14: Top: test signal T (blue) and network output signal T (red) in recurrent configuration on T; bottom: test signal B (blue) and network output signal B (red) in recurrent configuration on B

In Figure 3.15 the nonlinear functions of equations (3.11) are shown.

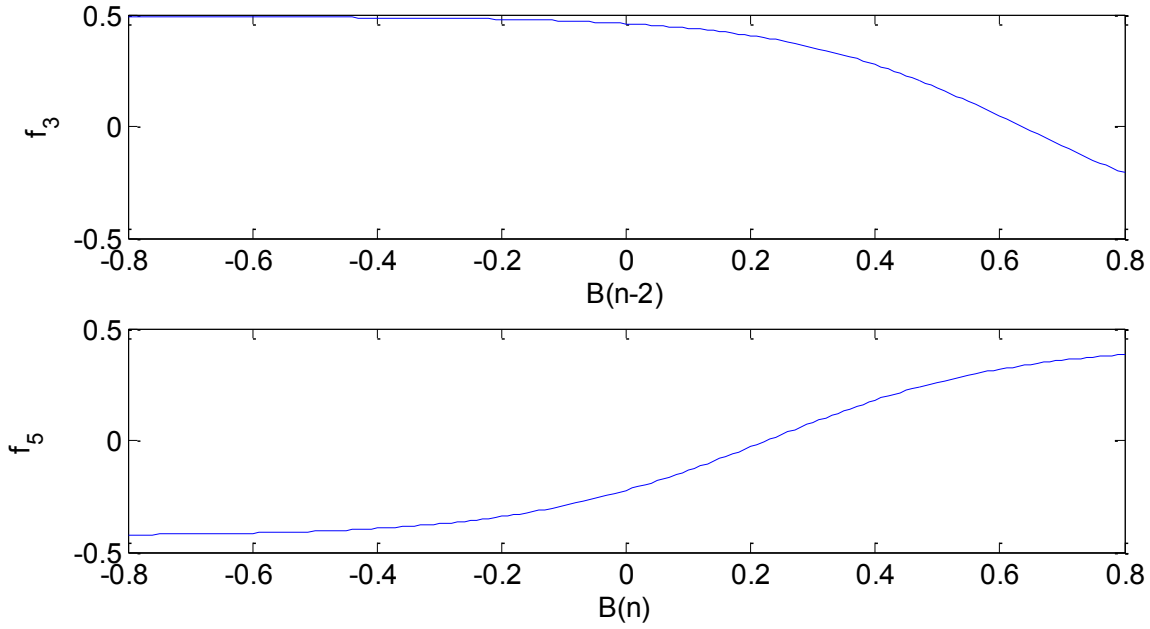

(a)

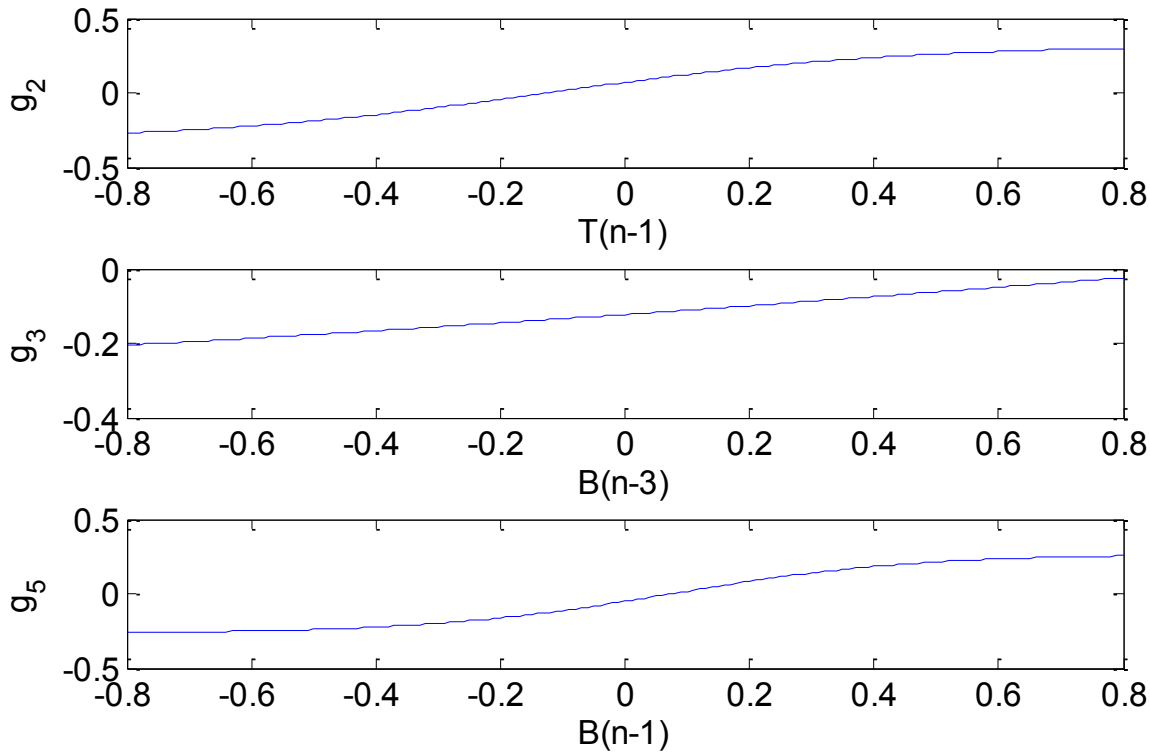

(b)

Figure 3.15: Nonlinear functions for equations (3.11): a) f_3, f_5 ; b) g_2, g_3, g_5

The identification has been repeated for a number of cases but the statistics is limited by the quality of the measurements available. The optimal configurations of the networks for the various cases in summarized in Table I.

Table I
Summary of the ansatzes found optimal for examples of Type I and Type III ELMs.

	f1	f2	f3	f4	f5	g1	g2	g3	g4	g5	l1	l2	h1
Pulse 79389 Type I ELMs	1	1	0	1	1	0	1	0	0	1	0	0	0
Pulse 79837 Type I ELMs	1	1	0	1	0	0	1	0	1	1	1	0	0
Pulse 79371 Type I ELMs	0	1	1	0	1	1	1	0	1	1	0	1	1
Pulse 79498 Type III ELMs	0	0	1	0	1	0	1	1	0	1	0	0	0

The results of the identification process indicate that there seems to be a systematic difference between the two types of ELMs. In particular, the Type III ELM analyzed is the only one which does not require f_2 (feedback on the temperature at time $n-1$); it is also the only case, which requires g_3 (feedback on the field at time $n-3$). The ansatzes of the Type I ELMs are not exactly identical but certainly much more similar to one another than to the Type III case. Of course the limited statistics available and the preliminary nature of the present studies do not allow drawing conclusions on the physics of the instabilities. On the other hand, these preliminary results indicate that RNNs are very powerful and they have the potential to identify complex instabilities in thermonuclear plasmas, provided measurements of acceptable quality are available.

The potential of recurrent neural networks, to identify complex dynamical systems, has been investigated. In addition to the case of synthetic signals, the RNNs have also been applied to experimental data. In particular the time evolution of the edge temperature and magnetic field due to Type I and Type III ELMs have been identified quite successfully with networks of the appropriate topology. The identification of experimental signals has proved to be quite challenging mainly because of two main factors: a) the complex dynamics of the instabilities b) the significant level of noise. Notwithstanding these difficulties, the results are quite encouraging. The long term

objective of this line of research consists of deriving quantitative information about the ELMs dynamics (both type I and type III) by investigating the topology of the networks more suited to identify them.

4

Identification of a stable LTI plant by using a predictor and a parallel model

This chapter is the result of a selected part of the work during my period at Yale where I had the pleasure to join the research team of Professor Narendra at the School of Engineering. As mentioned in Chapter 1, the need to investigate on new powerful identification techniques pushes the researcher towards new challenging areas. Firstly, a brief description of series parallel model and parallel model is introduced to underline the importance of the parallel models as a "true model" for identification purposes. Then results are shown for a second-order LTI system, whose dynamic is characteristic of a wide range of electronic circuits. The considerations and results here obtained want to pose the problem for future research development.

4.1 Series parallel model and parallel model

Let us start from the simplest identification problem, as described in [71]. Consider the identification problem of a plant described by first-order linear time-invariant differential equation with unknown coefficients a and b:

$$\dot{x}_p(t) = ax_p(t) + bu(t) \qquad (4.1)$$

The equilibrium state of the plant is assumed asymptotically stable $(a < 0)$ and the identification problem consists of the determination of a and b from the observed input-output pairs $u(t)$ and $x_p(t)$. For this purpose we take into account two different identification models (Figure 4.1): the parallel model and the series-parallel model (predictor). The input u and output $\hat{x}_p$ of parallel identification model has the following structure

$$\dot{\hat{x}}_p(t) = \hat{a}(t)\hat{x}_p(t) + \hat{b}(t)u(t) \qquad (4.2)$$

while for the series parallel model we obtain

$$\dot{\hat{x}}_p(t) = a_m\hat{x}_p(t) + [\hat{a}(t) - a_m]x_p(t) + \hat{b}(t)u(t) \qquad a_m < 0 \qquad (4.3)$$

where $\hat{a}(t)$ and $\hat{b}(t)$ are the estimates of a and b at time t.

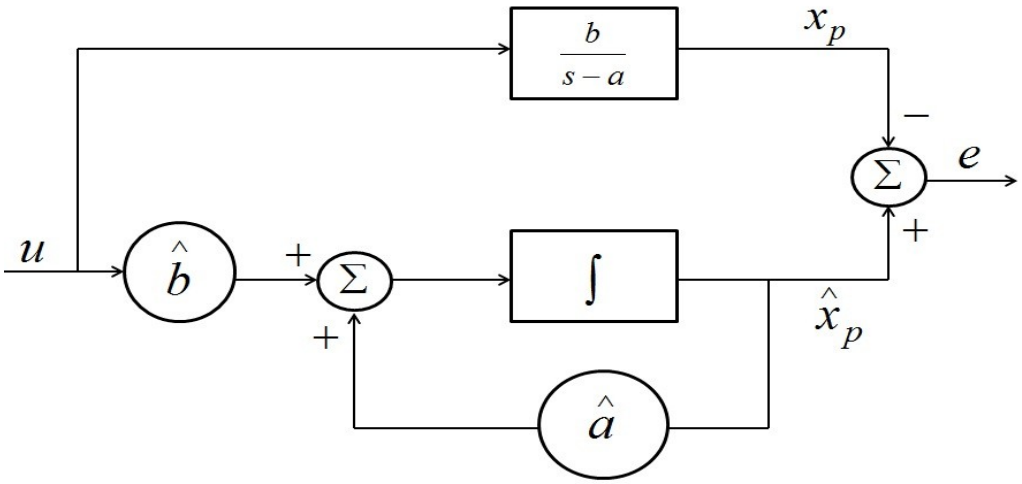

(a)

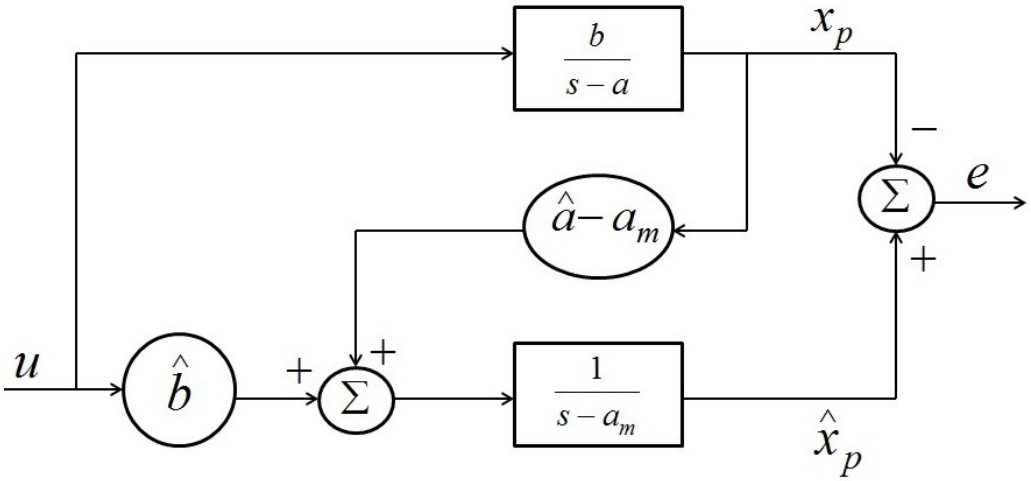

(b)

Figure 4.1: Two different identification models: a) parallel model; b) series parallel model.

By observing the structure of the two different models one notices that the series parallel model it is not a true model but it is a predictor that requires to be fed by the output of the plant $x_p(t)$ to produce the estimation $\hat{x}_p(t)$. On the contrary the parallel identification model can be considered a "true model" that after the identification phase can be used independently from the plant to reproduce its dynamic.

4.2 Statement of the problem

Let us focus our attention on discrete-time systems. Given a discrete-time plant Σ_p (stable with state accessible) described by the state equations:

$$x_p(k+1) = A_p x_p(k) + bu(k) \qquad (4.3)$$

where $x_p(\cdot) : R^+ \to R^n$, $u(\cdot) : R^+ \to R$. $A_p \in R^{n \times n}$ and $b \in R^n$ are in a companion form. The elements of last row of the matrix A_p are $\vartheta_p^T = [a_{p(1),} a_{p(2),} \dots, a_{p(n)}]$ and are assumed to be unknown. $b = [0, \dots, 0, 1]^T$ and the input u is bounded. The problem is the identification of the plant described by (4.3) by using different models. Specifically a series-parallel model (predictor) and a parallel model are studied for this purpose. The aim of the predictor is providing an estimation of the plant parameters to the parallel model. The identification problem is initialized by using the only predictor, then according to a switching criterion from the predictor to the parallel model, only the latter will be used for the plant identification. A predictor with a stable adaptive law for the estimation of ϑ_p^T is presented in section 4.3. The switching criterion is discussed in section 4.4. A parallel model is presented in section 4.5. The aim of the activity is evaluate the use of a parallel model for the plant identification. Since the parallel model can perform the identification only if its parameters lie in a neighborhood of those of the plant the first step of the procedure consists of using a predictor to obtain a first plant estimation and then switching to the parallel model.

4.3 Identification by using a Series-Parallel-Model (Predictor)

An identification model Σ_I, described by the following equation is set up to identify ϑ_p :

$$x_I(k+1) = A_m x_I(k) + [A_I(k) - A_m] x_p(k) + bu(k) \qquad (4.4)$$

where $A_I(k)$ is a matrix in companion form, whose last row $\vartheta_I^T(k) = [a_{I(1)}(k), a_{I(2)}(k), \dots, a_{I(n)}(k)]$ is the estimate of the plant parameters. A_m is a stable matrix known. Let us indicate the parameter error with $\Phi(k) = A_I(k) - A_p$ and the identification error with $e_I(k) = x_I(k) - x_p(k)$. The error equation can be written:

$$e_I(k+1) = A_m e_I(k) + \Phi(k) x_p(k) \quad (4.5)$$

The following stable adaptive law assures the boundedness of both the identification error and the parameter error [72]:

$$\Phi(k+1) = \Phi(k) - \frac{\mathcal{E}(k)x_p^T(k)}{1+x_p^T(k)x_p(k)} \quad (4.6)$$

where $\mathcal{E}(k) = e_I(k+1) - A_m e_I(k)$.

The adaptive law (4.6) can be rewritten as:

$$\vartheta_I(k+1) = \vartheta_I(k) - \frac{\bar{\mathcal{E}}(k)x_p^T(k)}{1+x_p^T(k)x_p(k)} \quad (4.7)$$

where $\bar{\mathcal{E}}(k)$ is the last row of $\mathcal{E}(k)$.

4.4 Switching criterion

In this section the criteria to switch from the predictor to the parallel model during the identification procedure is described. Let us define the following error that takes into account the sum of the square identification error into a preset time window T :

$$E_I(k) = \sum_{j=k-T+1}^{k} e_i^T(j)e_i(j) \qquad \forall\, k \geq T \qquad (4.8)$$

where $e_i(j)$ is the identification error of the series parallel model at time j. The parallel model starts at $k = \bar{k}$ when

$$E_I(\bar{k}) < \sigma \qquad (4.9)$$

where $\sigma \in R$ is a preset threshold and $\bar{k}$ is the switching time from the series parallel model to the parallel model. It means that for $k \leq \bar{k}$ only the predictor will be used for the plant identification while for $k > \bar{k}$ only the parallel model with its own adaptive law will be used for identification purposes. The smaller is σ the better is the parameters estimation provided by the predictor to the parallel model.

4.5 Identification by using a parallel model

An identification model Σ_{pm} is described by the following state equations:

$$x_{pm}(k+1) = A_{pm}(k)x_{pm}(k) + bu(k) \qquad (4.10)$$

where $A_{pm}(k)$ is a matrix in a companion form such that the last row is $\vartheta^T(k) = [a_1(k), a_2(k), \dots, a_n(k)]$. The following error equation can be written:

$$e_{pm}(k+1) = A_p e_{pm}(k) + \Phi_{pm}(k)x_{pm}(k) \quad (4.11)$$

where $e_{pm}(k) = x_{pm}(k) - x_p(k)$ and $\Phi_{pm}(k) = A_{pm}(k) - A_p$.

Let us define $\bar{\bar{\varepsilon}}(k+1)$ as:

$$\bar{\bar{\varepsilon}}(k+1) = \bar{e}_{pm}(k+1) - \vartheta^T(k)e_{pm}(k) \qquad (4.12)$$

where $\bar{e}_{pm}(k+1)$ is the last row of $e_{pm}(k+1)$. Using the projection algorithm proposed in [72], the following difference equation can be used to adjust $\vartheta(k)$ for the parallel model:

$$\vartheta(k+1) = \vartheta(k) - \frac{x_p(k)\bar{\bar{\varepsilon}}(k+1)}{1 + x_p(k)x_p^T(k)} \qquad (4.13)$$

Alternatively, in order to damp the oscillations during the convergence the following difference equation can also been used:

$$\vartheta(k+1) = \vartheta(k) - \frac{1}{l}\sum_{j=k-l+2}^{k+1} \varphi(k+1) \qquad \forall\, k:\ k+1 = nl \qquad (4.14)$$

where $\varphi(k+1) = \frac{x_p(k)\bar{\bar{\varepsilon}}(k+1)}{1+x_p(k)x_p^T(k)}$. Equation (4.14) can be used to adjust $\vartheta(k)$ every l steps taking into account the previous values of φ. This allows a smoother behavior during the parameter convergence.

4.6 Simulation results

Let us consider a second order plant described by (4.3) , with $A_p(k) = \begin{bmatrix} 0 & 1 \\ 0.1 & 0.2 \end{bmatrix}$ and initial conditions $x_p(1) = [0.1, 0.1]^T$. $u(k) = \sin\left(\frac{\pi k}{10}\right) + \sin\left(\frac{3\pi k}{10}\right)$, $b = [0,1]^T$.

Let us consider a predictor (4.4) with $A_m(k) = \begin{bmatrix} 0 & 1 \\ -0.3 & -0.3 \end{bmatrix}$ and initial conditions $x_I(1) = x_p(1)$. Initial conditions for $\vartheta_I(1) = [0.3,0.3]^T$.

The following cases with different switching parameters have been considered:

case 4.6.1 : According to the switching criteria introduced in section 4.4 the following parameters have been chosen: $T = 10, \sigma = 0.001$.

case 4.6.2 : According to the switching criteria introduced in section 4.4 the following parameters have been chosen: $T = 10, \sigma = 0.1$.

case 4.6.3 : According to the switching criteria introduced in section 4.4 the following parameters have been chosen: $T = 10, \sigma = 10$.

case 4.6.4 : In this case no predictor has been used and the only constraint for the parallel model is that the initial conditions for ϑ are such that $A_{pm}(1)$ is stable. Specifically $\vartheta(1) = [0.3575, 0.5155]^T$. Initial conditions: $x_{pm}(1) = x_p(1)$.

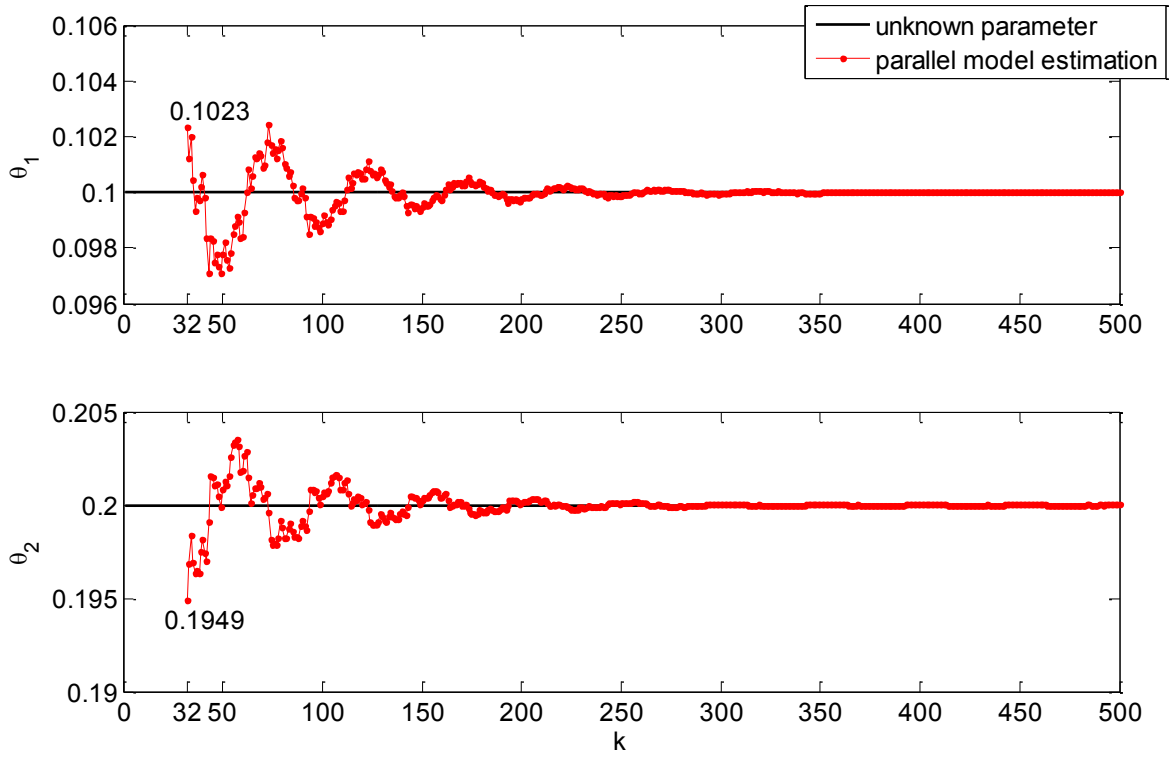

Figure 4.2: Case 4.6.1, plant parameter estimation by using the parallel model in a neighborhood of the plant parameters. The parallel model estimation starts at k=32 from $\vartheta(1) = [0.1023, 0.1949]^T$.

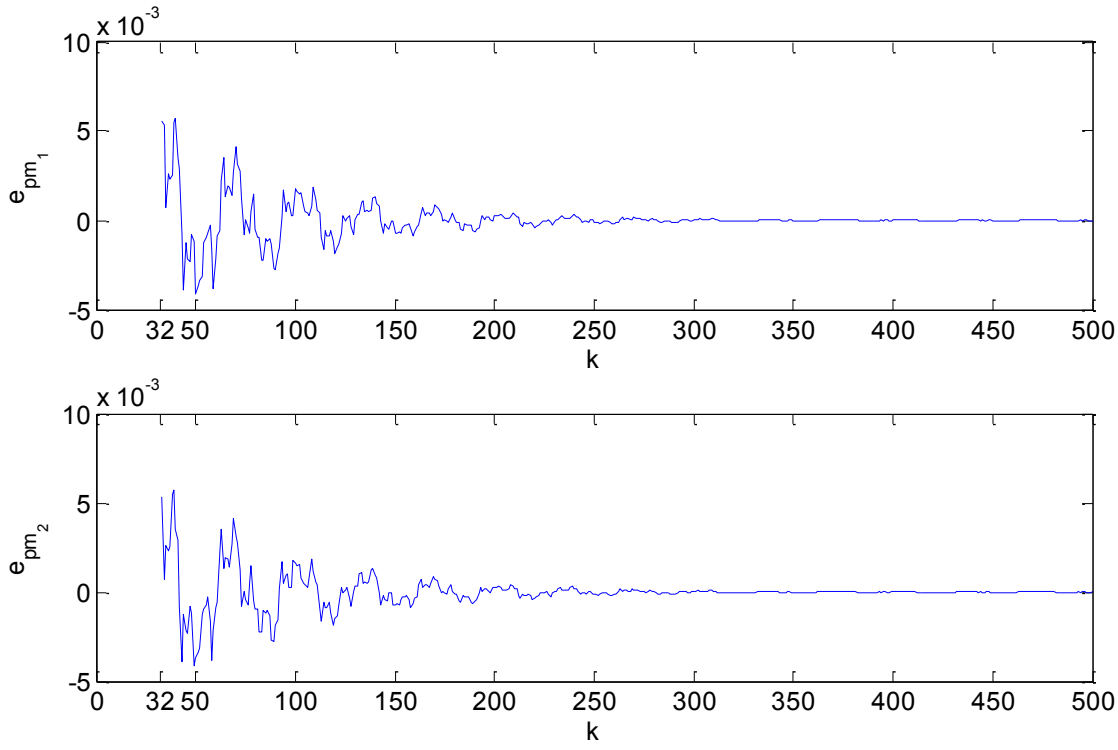

Figure 4.3: Case 4.6.1, identification error between the parallel model and the plant.

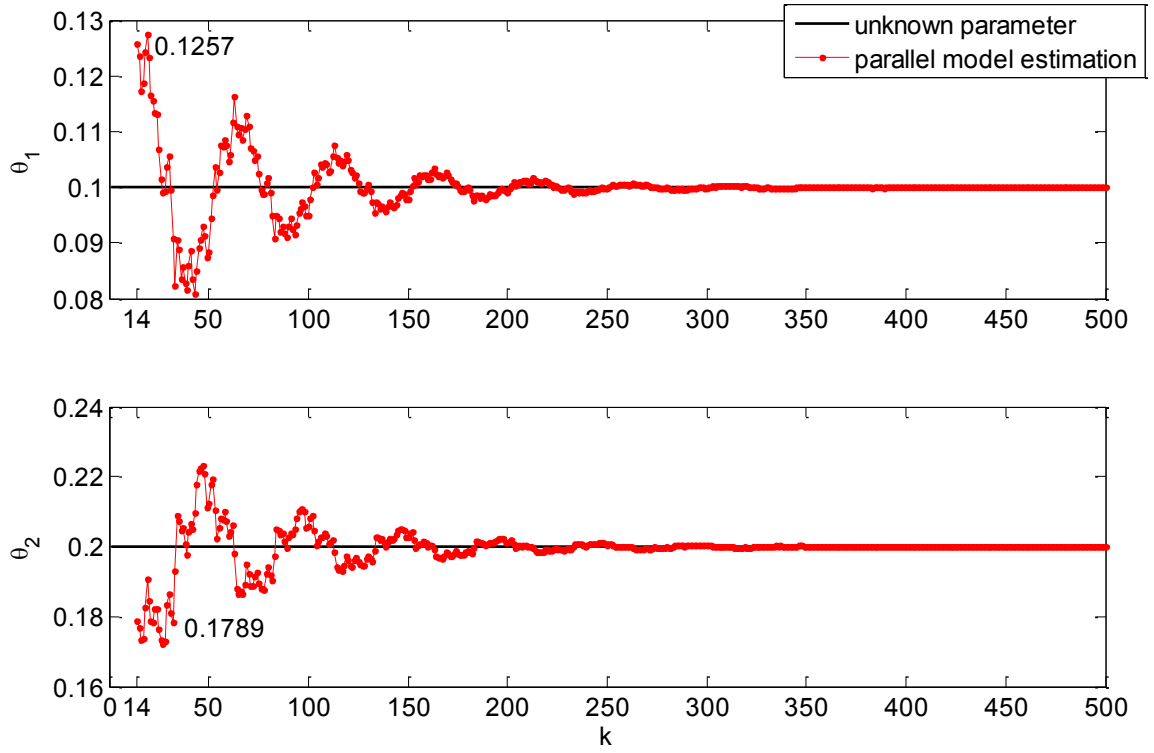

Figure 4.4: Case 4.6.2, plant parameter estimation by using the parallel model in a neighborhood of the plant parameters. The parallel model estimation starts at k=14 from $\vartheta(1) = [0.1257, 0.1789]^T$.

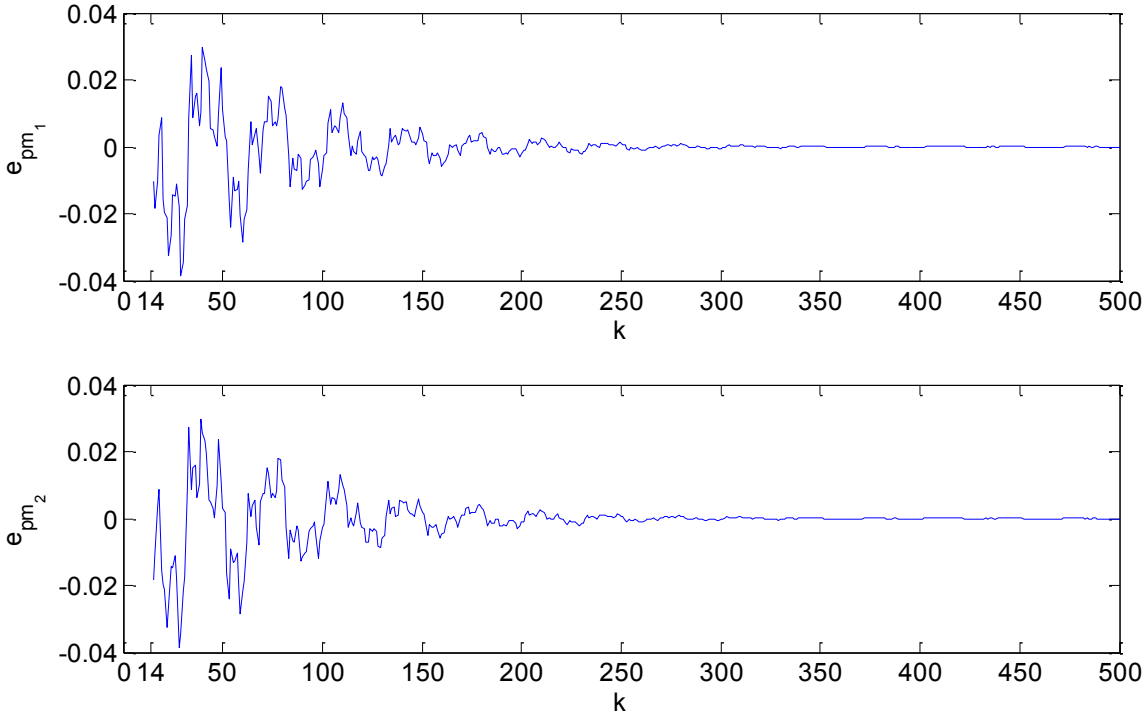

Figure 4.5: Case 4.6.2, identification error between the parallel model and the plant.

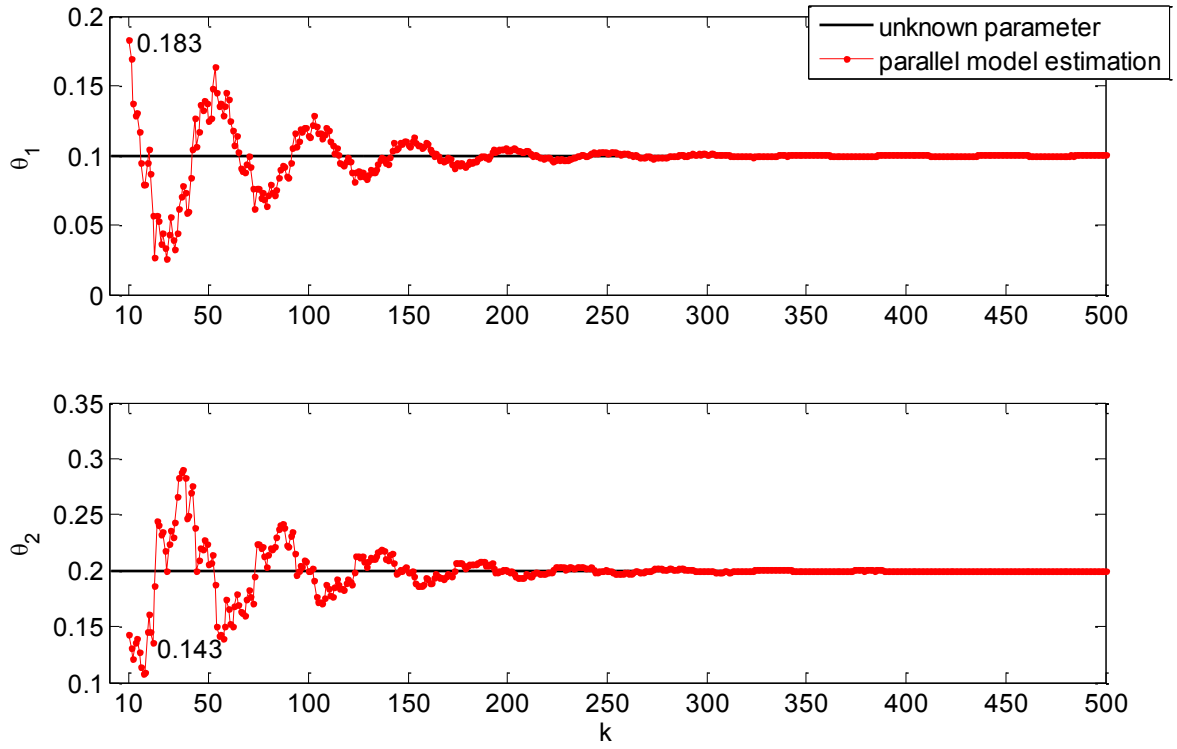

Figure 4.6: Case 4.6.3, plant parameter estimation by using the parallel model in a neighborhood of the plant parameters. The parallel model estimation starts at k=10 from $\vartheta(1) = [0.183, 0.1431]^T$.

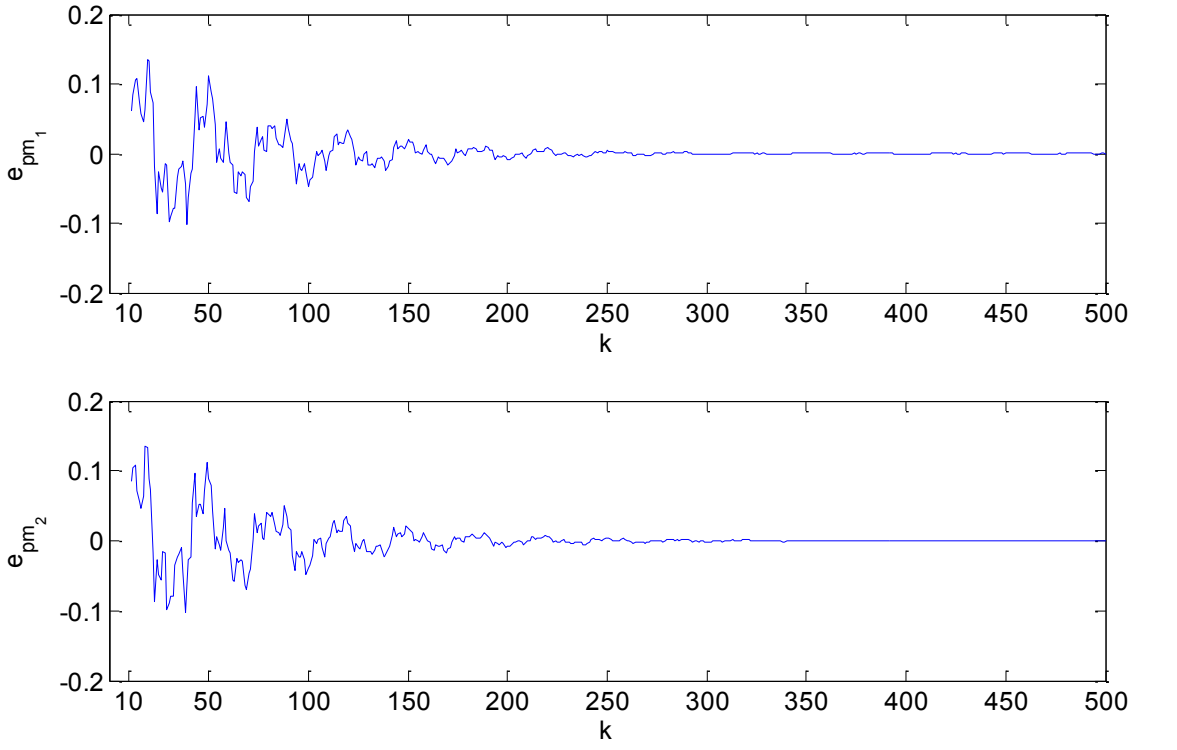

Figure 4.7: Case 4.6.3, identification error between the parallel model and the plant.

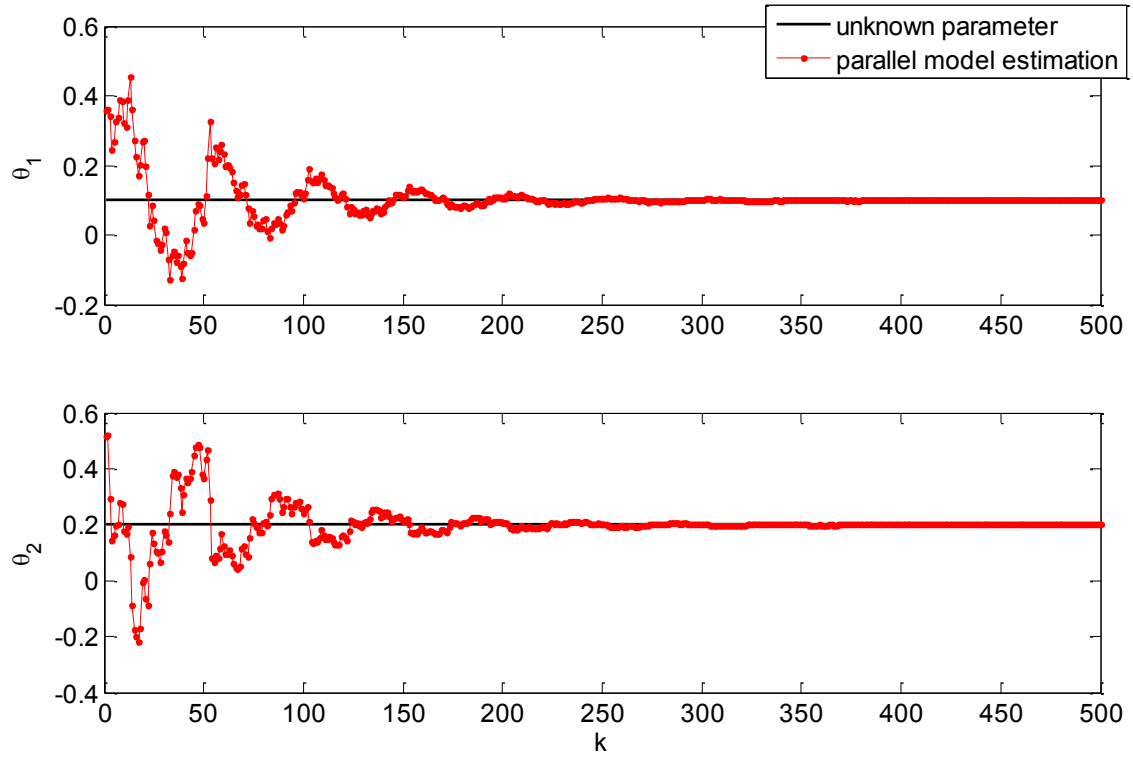

Figure 4.8: Case 4.6.4, plant parameter estimation by using the parallel model without the predictor. $\vartheta(1) = [0.3575, 0.5155]^{\mathrm{T}}$.

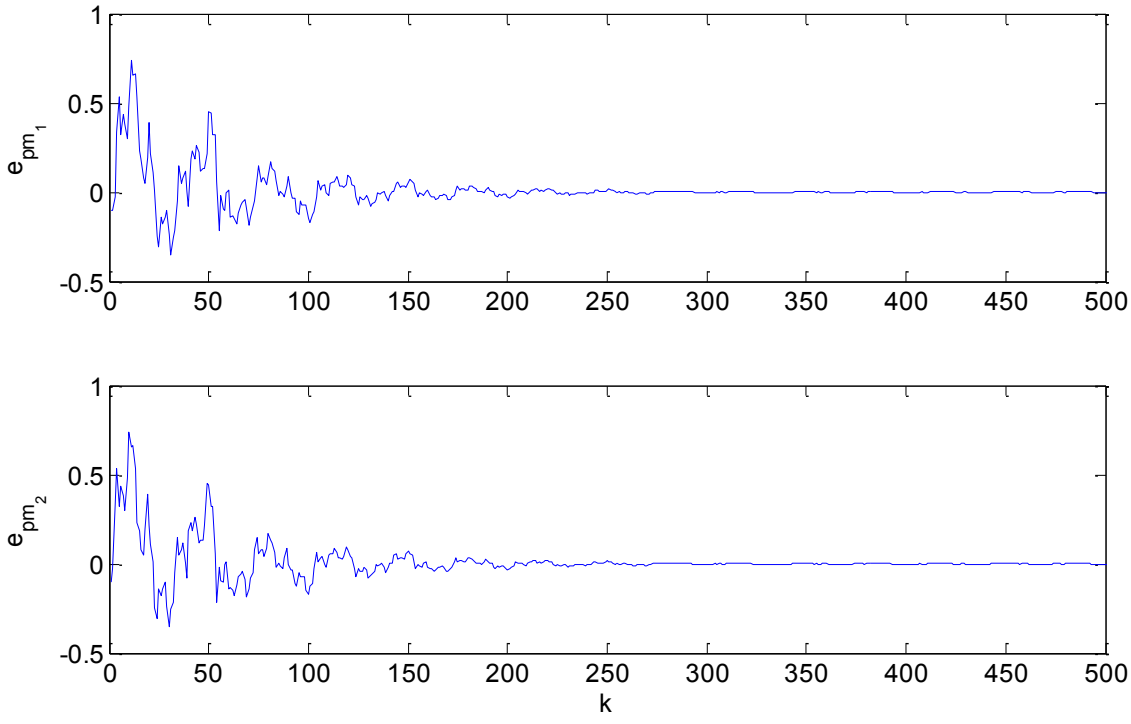

Figure 4.9: Case 4.6.4, identification error between the parallel model and the plant.

Experiments 4.6.1 - 4.6.4 show that the better is the estimation provided by the predictor at the time $\bar{k}$ the better will be the parallel model identification for $k > \bar{k}$. Moreover, the larger is σ the smaller is the switching time $\bar{k}$ from the predictor to the parallel model. The previous experiments show how the parallel model is able to identify the stable plant both starting from a good estimation of the plant provided by the series parallel model and also in the case (4.6.4) in which there is no series parallel model with the only constraint that the initial parameters of the parallel model $\vartheta(1)$ are inside the stability region. These results can be used as a starting point to assess the use of the parallel model identification scheme in a wide range of application in which the designer requires a true model instead of a predictor.

4.7 Considerations on the applied procedure to derive the adaptive law for the parallel model

The idea behind equation (4.13) used to adjust the parallel model parameters vector ϑ in section 4.5 lies on an intriguing procedure. Starting from the consideration that the plant is unknown while the parallel model parameters are known, the problem is how to adjust the parallel model parameters vector ϑ to converge towards ϑ_p. Let us treat, theoretically, the parallel model as a reference model and our target is that the plant follows the "reference model". Then, the problem becomes a standard control problem. At each step, once we calculate the quantity $\Delta\phi$ of which we have to move the plant towards the reference model (Figure 4.10) we move the parallel model of the opposite quantity $(-\Delta\phi)$.

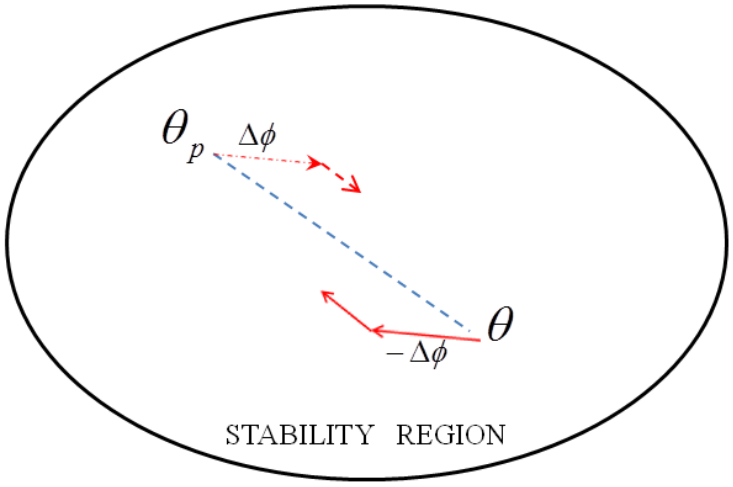

Figure 4.10: base idea to adjust the parallel model parameter vector ϑ.

Let us define $\phi^T(k) = [a_1(k) - a_{p(1)}, \dots, a_n(k), \dots, a_{p(n)}]$, then we can write:

$$x_p(k+1) = A_{pm}(k)x_p(k) - b\phi^T(k)x_p(k) + bu(k) \qquad (4.15)$$

and we can calculate:

$$e_c(k+1) = x_p(k+1) - x_{pm}(k+1) = A_{pm}(k)e_c(k) - b\phi^T(k)x_p(k) \qquad (4.16)$$

then

$$\mathcal{E}_c(k+1) = e_c(k+1) - A_{pm}(k)e_c(k) = -b\phi^T(k)x_p(k) \qquad (4.17)$$

and

$$\Delta\phi(k) = -\frac{x_p(k)\overline{\overline{\mathcal{E}_c}}(k+1)}{1+x_p(k)x_p^T(k)} = \frac{x_p(k)\bar{\bar{\mathcal{E}}}(k+1)}{1+x_p(k)x_p^T(k)} \qquad (4.18)$$

where $\overline{\overline{\mathcal{E}_c}}(k+1)$ is the last row of $\mathcal{E}_c(k+1)$.

5

Concluding remarks

This thesis focused on the study of nonlinear oscillations in high power systems in two reference frameworks (systems/devices used to sustain plasma fusion and power electronic modules). The systems studied have been analysed, identified and modeled using different approaches.

The modeling of macroscopic JET plasma instabilities has been treated by proposing both data-driven modeling approaches and model-based ones. The former involved empirical models described by mathematical equations that are not derived from the physical knowledge of the system but from analysis of time series data using neural networks. The motivation that pushed toward the use of this approach is twofold: the lack of a detailed knowledge of the system and the availability of a considerable amount of data describing the problem.

In the same context, a model-based approach has also been proposed to face with the modeling problem from a different perspective: the study of a mathematical model capable of reproducing plasma instabilities behavior through the experimental observations of a rescaled electronic analogous.

Concerning the power electronics framework, the high power density characterizing power electronic modules for industrial applications makes of primary importance the investigation on thermal behavior of these devices. For this purpose, an integrated procedure starting from FE models validated by experimental data has been introduced. In the proposed methodology FE models are used to provide source information to a lumped parameter modeling that allows a fast prototyping of the devices.

The proposed methodology is based on the assumption that the heat transfer problem can be assumed to be linear and the thermal impedances approach can be therefore used. The approach used is general as it can be used to extract the thermal networks either from FE models or experimental data of thermal impedances. In fact, the use of FE model is only finalized to get the thermal impedances curves to derive lumped parameter models, so it will be used only once. Then, it is possible to simulate the module thermal behavior by means of a generic circuit simulator at least at some "critical" points in a faster way than a FE model which needs of a specific FEM tool. Secondly, the lumped parameter thermal model obtained can be easily integrated with a power module electrical model.

In the last chapter a study on new identification techniques based on parallel identification models is also proposed for discrete-time systems. This study has been motivated by the importance of investigating on new identification methodologies that lie on the implementation of a true identification model. The results obtained can be used to set the problem for new research developments.

References

[1] D. C. Hamill, S. Banerjee and G. C. Verghese, *Nonlinear phenomena in power electronics*, New York, IEEE Press, 2001.

[2] A.M. Trzynadlowsky, *Introduction to Modern Power Electronics*, Wiley 2010.

[3] H.Bai, C. Mi, *Transients of Modern Power Electronics*, Wiley 2011.

[4] G.Revel, D.M. Alonso, J.L. Moiola, "Bifurcation Theory applied to the analysis of power systems", *Revista de la union matematica Argentina*, Vol. 49, no.1, 2008.

[5] J.H.Deane and D.C Hamill, "Improvement of power supply EMC by chaos", *Electronics Letters*, vol.32, no.12, p. 1045, 1996.

[6] S. Iqbal, M. Ahmed, S.A. Qureshi, "Investigation of Chaotic Behavior in DC-DC Converters", *World Academy of Science, Enginnering and Technology* 33, 2007.

[7] A. Buscarino, L. Fortuna, M, Frasca, M. Iachello, V.T. Pham, "Robustness to noise in synchronization of networks motifs: experimental results"*, Chaos* 22, 043106, 2012.

[8] E. Ott, C. Grebogi and J.A. Yorke, "Controlling Chaos"*, Physics Review Letters*, vol. 64, no. 11, pp. 1196-1199, 1990.

[9]W.L. Ditto, S.N. Rauseo and M.L. Spano, "Experimental control of chaos"*, Physics Review Letters*, vol. 65, no. 26, pp. 3211-3214, 1990.

[10] T. Shinbrot, C. Grebogi, E. Ott and J.A. Yorke, "Using small perturbations to control chaos", *Nature*, vol. 363, no. 6428, pp. 411-417, 1993.

[11] G.Podder, K. Chakrabarty, S. Banarjee, "Experimental control of chaotic behavior of buck converter", *IEEE Trans. on Circuits and Systems* I vol, 42, no.8, pp 100-101, 1995.

[12] D.C Hamill, "Power Electronics: A field rich in nonlinear dynamics", *Proc. 3rd Int. Specialists Workshop on Nonlinear Dynamics of Electronic Systems*, 1995.

[13] S. Banerjee, J.A .Yorke, C. Grebogi, "Robust chaos", *Phisycal Review Letters*, vol. 80, 1998.

[14] J.L. Marrero, J. M. Font, G.C. Verghese, "Analysis of the chaotic regime for dc-dc converters under current mode control", *IEEE Power Electronics Specialists Conference*, 1996.

[15] Wesson J. *Tokamaks* 3rd edition, 2004 (Oxford: Clarendon).

[16] www.iter.org

[17] T.R. Boehly, D.L Brown, R.S Craxton, R.L Keck, J.P Knauer, J.H Kelly, T.J Kessler, S.A Kumpman, S.J Loucks, S.A Letzring, F.J Marshall, R.L McCrory, S.F.B Morse, W Seka, JM Sources, C.P Verdon, "Initial performance results of the OMEGA laser system", *Optics Communications*, Volume 133, Issues 1-6, January 1997, pp. 495-506

[18] E. Bertolini, T. Boniceli, D. Chiron, A. Stantagiustina, "Power Electronics Systems at JET: Objectives and Operational Experience", Preprint (JET-P(95)11).

[19] P.Fu, Z.Z. Liu, G. Gao, L. Yang, Z.Q. Song, L.W. Xu, J. Tao and X.N. Liu, "Power Supply system of EAST -Superconducting Tokamak", 5th *IEEE Conference on Industrial Electronics and Applications*.

[20] A. Murari, P. Arena, A. Buscarino, L. Fortuna, M. Iachello, & JET-EFDA Contributors, "On the Identification of Instabilities with Neural Networks on JET", *Nuclear Instruments and Methods in Physics Research Section A: Accellerators, Spectrometers, Detectors and Associated Equipment*, Volume 720, August 2013, pp. 2-6.

[21] W. Arter, "Symmetry Constraints on the Dynamics of Magnetically Confined Plasma", *Physical review letters* 102, 195004, 2009.

[22] A. Buscarino, L. Fortuna, M. Frasca, M. Iachello, "A new oscillator scheme for analog modeling", *European Conference on Circuit Theory and Design*, Dresden, 8 -12 September 2013.

[23] R. Genesio and A. Tesi, "Harmonic Balance methods for the analysis of chaotic dynamics in nonlinear systems", *Automatica*, 28, pp. 531-548, 1992.

[24] A. Gelb and W. E. Vander Velde, *Multiple-input describing functions and nonlinear system design*, McGraw-Hill Book Co., 1968.

[25] D.P. Atherton, *Nonlinear control engineering*, Van Nostrad Reinhold Co. Ltd., Wokingham, UK, 1982

[26] J. J. E. Slotine and W. Li, *Applied nonlinear control*, Prectice-Hall International editions, London, UK, 1991.

[27] L. Fortuna, M. Frasca and M.G. Xibilia, *Chua's Circuit Implementations: Yesterday, Today, Tomorrow,* World Scientific, 2009.

[28] A. Baranyi and L. O. Chua, "Dynamic Model for the Analog Multiplier", *IEEE Transactions on Circuits and Systems* 29, pp. 65.76, 1982.

[29] B. Gilbert, "A high-performance monolithic multiplier using active feedback", *IEEE Journal of Solid-State Circuits* 9, pp. 364-373, 1974.

[30] R. Caponetto, L. Fortuna, G. Manganaro, M.G. Xibilia, "Synchronization-based nonlinear chaotic circuit identification", *Proc. SPIE 2612, Chaotic Circuits for Communication*, 48, 1995.

[31] M. Iachello, V. De Luca, G. Petrone, N. Testa, L. Fortuna, G. Cammarata, S. Graziani, M. Frasca, "Lumped Parameter Modeling for Thermal Characterization of High Power Modules", *IEEE Trans. Comp. Packag. Techn.*, 2014.

[32] J. Kolar, J. Biela, S. Waffler, T. Friedli, and U. Badstuebner, "Performance trends and limitations of power electronic systems", *in Proc. Conf. Integr. Power Electron. Syst.Rec. Nuremberg*, Mar. 2010, pp. 17-36.

[33] D. Boroyevich, F. Wang, R. Burgos, R. Lai, and S. Wang, "High-density system integration for medium power applications", in *Proc. Conf. Integr. Power Electron. Syst. Rec.,* Nuremberg, Mar. 2010, pp. 47-56.

[34] A. Bryant, N.A. Parker-Allotey, D. Hamilton, I. Swam, P. A. Mawby, T. Ueta, T. Nishijima, and K. Hamada, "A Fast Loss and Temperature Simulation Method for Power Converters, Part I: Electrothermal Modeling and Validation", *IEEE Transactions on Power Electronics*, vol. 27, no.1, January 2012.

[35] I. Swan, A. Bryant, P. A. Mawby, T. Ueta, T. Nishijima, and K. Hamada, "A Fast Loss and Temperature Simulation Method for Power Converters, Part II: 3-D Thermal Model of Power Module", *IEEE Transactions on Power Electronics*, vol. 27, no.1, January 2012

[36] L. Fortuna, M. Frasca, G. M. Rivituso, "An innovative method for thermal characterization of automotive electronic devices based on CNNs", *IEEE Trans. Instrumentation and Measurement*, vol. 59, no. 6, pp.1671-1677, 2010.

[37] S. Carubbelli, Z. Khatir, and F. Lecoq, "Experimental validation of a thermal modelling method dedicated to multichip power modules in operating conditions", *Microelectronics Journal* 34, pp.1143–1151, 2003.

[38] Z. Khatir, S. Lefebvre, "Thermal Analysis of Power Cycling Effects on High Power IGBT Modules by the Boundary Element Method", *Semiconductor Thermal Measurement and Management*, *Seventeeth Annual IEEE Symposius*, 2001.

[39] C-S. Yun, P. Malberti, M. Ciappa, and W. Fichtner, "Thermal Component Model for Electrothermal Analysis of IGBT Module System", *IEEE Transactions on Advanced Packaging*, vol. 24, no. 3, August 2001

[40] U. Drofenik, D. Cottet, A. Musing, J-M Meyer and J.W. Kolar, "Modelling the Thermal Coupling between Internal Power Semiconductor Dies of a Water-Cooled 3300V/1200A HiPak IGBT Module", *Proceedings of Power Conversion and Intelligent Motion Conference*, 2007.

[41] Z. Jiang, X. Liu, S. Jiao and J. Han, "Investigation of the Temperature Character of IGBT Failure Mode based the 3-D Thermal – Electro Coupling FEM , A*dvanced Materials Research* Vols, 655-657, pp 1576-1580, 2013.

[42] U. Drofenik, D. Cottet, A. Musing, J-M. Meyer and J. W. Kolar, "Computationally Efficent Integration of Complex Thermal Multi-Chip Power Module Models into Circuit Simulators", *Power Conversion Conference*, Nagoya, 2007.

[43] N. Y. A. Shammas, M. P. Rodriguez, F. Masana, "A simple method for evaluating the transient thermal response of semiconductor devices", *Microelectronics Reliability* 42, pp. 109-117, 2002.

[44] F.N. Masana, "A new approach to the dynamic thermal modelling of semiconductor packages", *Microelectronics Reliability* 41 (2001) 901-912.

[45] Z. Khatir, S. Carubelli and F. Lecoq, "Real-Time Computation of Thermal Constraints in Multichip Power Electronics Devices", *IEEE Transaction on components and packaging technologies*, Vol. 27, No. 2, June 2004.

[46] R. W. Lewis, K. Morgan, H. R. Thomas and K. N. Seetharamu, *The Finite Element Method in Heat Transfer Analysis*. New York: Wiley, 1996.

[47] Y. A. Cengel, *Heat Transfer: A practical Approach*, Mcgraw-Hill, 2nd edition, 2002.

[48] http://www.cise.ufl.edu/research/sparse/umfpack/

[49] B. D. O. Anderson and S. Vongpanitlerd. *Network Analysis and Synthesis: A Modern Systems Approach*. Dover Publications, New York, 2006

[50] W.K. Chen, *The circuits and filters handbook. Passive, active, and digital filters*, CRC Press (2009).

[51] J. A. Nelder and R. Mead, "A simplex method for function minimization", *The Computer Journal* 7 (4): 308-313, 1965.

[52] J. C. Lagarias, J. A. Reeds, M. H. Wright, and P. E. Wright, "Convergence Properties of the Nelder-Mead Simplex Method in Low Dimension", *Siam J. Optim* Vol. 9, No. 1, pp. 112-147, 1998

[53] AC Hindmarsh, P.N Brown, K.E Grant, S.L. Lee, R. Serban, D.E. Shumaker, and C.S. Woodward, , "SUNDIALS: Suite of Nonlinear and Differential/Algebraic Equation Solvers", *ACM Trans. Math. Software*, 31, pp. 363-396, 2005.

[54] Analysis Tech, http://www.analysistech.com

[55] J.W.Sofia, *Fundamentals of Thermal Resistance Measurament*, Analysis Tech, 1995.

[56] L. Codecasa, D. D'Amore, and P. Maffezzoni, "An Arnoldi Based Thermal Network Reduction Method for Electro-Thermal Analysis", *IEEE Trans. Comp. Packag. Trechnol.*, vol.26, no. 1, pag 186-192, Mar. 2003

[57] L. Codecasa, D. D'Amore, and P. Maffezzoni, "Compact Thermal networks for modeling packages", *IEEE Trans. Comp. Packag. Technol*, vol. 27, no. 1, Mar. 2004

[58] L Fortuna, M. Frasca, *Optimal and Robust Control: Advanced Topics with MATLAB*, CRC press (2012).

[59] C. A. Desoer, E. S. Kuh, *Basic Circuit Theory*, McGraw-Hill, 2009

[60] A. Murari, A. Buscarino, L. Fortuna, M. Frasca, M. Iachello, G. Mazzitelli, "Identifying JET instabilities with Neural Networks", *Electrotechnical Conference (MELECON)*, Tunis, 25-28 March 2012.

[61] B. Yegnanarayana, *Artificial Neural Networks*. New Delhi, India: Prentice-Hall India,1999.

[62] J. Hopfield, "Artificial neural networks," *IEEE Circuits Devices Mag*. 4, pp 3–10 Sep. 1988.

[63] C.M. Bishop, *Neural Networks for Pattern Recognition*. Clarendon Press, Oxford, 1995.

[64] K Hornik, M Stinchcombe, H White, "Multilayer feedforward networks are universal approximators", *Neural networks*, vol.2, pp. 359-366, 1989.

[65] K.S. Narendra and K. Parthasarathy, "Identification and control of dynamical systems using neural networks", *IEEE Trans. Neural Networks*, vol.1, pp. 4-27, Mar. 1990.

[66] G.Cybencko, "Approximation by superpositions of a sigmoidal function", *Mathematics of control, signals and systems* vol 2, pp. 203-314, 1989.

[67] D. Patané, A. Murari, G. Vagliasindi, P. Arena, D. Mazon, V. Caloone, "Full Identification of Ordinary Differential Equations by means of Neural Networks", *IEEE Transactions on Neural Networks*, Submitted for publication.

[68] G. Napoli, M. G. Xibilia, "Soft Sensor design for a Topping process in the case of small datasets", *Computers & Chemical Engineering* 35, pp. 2447-2456, 2011.

[69] L. Fortuna, A. Rizzo, M. Sinatra, M.G. Xibilia, "Soft Analyzers for a Sulfur Recover Unit", *Control Engineering Practice* 11, pp. 1491-1500, 2003.

[70] S. Haykin, *Neural Networks and Learning Machines*, Pearson International Edition, London 2009.

[71] K. S. Narendra and A. M. Annaswamy, *Stable Adaptive Systems*, Englewood Cliffs, NJ: Prentice-Hall, 1989

[72] G. C. Goodwin and K. S. Sin. *Adaptive Filtering Prediction and Control*. Prentice-Hall, Inc., Englewood Cliffs, New Jersey 07632, 1984.

Personal publications

M. Iachello, V. De Luca, G. Petrone, N. Testa, L. Fortuna, G. Cammarata, S. Graziani, M. Frasca, "Lumped Parameter Modeling for Thermal Characterization of High Power Modules", *IEEE Transactions on Components, Packaging and Manufacturing Technology*, vol. 4, pp. 1613-1623, October 2014.

A. Buscarino, L. Fortuna, M. Frasca, M. Iachello, A new oscillator scheme for analog modeling, European Conference on Circuit Theory and Design, Dresden, 8-12 September 2013.

A. Murari, P. Arena, A. Buscarino, L. Fortuna, M. Iachello, "On the identification of instabilities with Neural Networks on JET", *Nuclear Instruments and Methods in Physics Research A*, vol. 720, pp. 2-6, August 2013.

M. Iachello, "On the investigation of lumped parameter models for thermal characterization of high power modules", 10th International Conference On Informatics in Control, Automation and Robotics, Doctoral Consortium, Reykjavik, 29-31 July 2013.

A. Buscarino, L. Fortuna, M. Frasca, M. Iachello, V. T. Pham, "Robustness to noise in synchronization of network motifs: experimental results", *Chaos* 22, 043106, October 2012.

A. Murari, A. Buscarino, L. Fortuna, M. Frasca, M. Iachello, G. Mazzitelli, "Identifying JET instabilities with Neural Networks", Electrotechnical Conference (MELECON), Tunis, 25-28 March 2012.

A. Murari, P. Arena, A. Buscarino, L. Fortuna, M. Iachello, "On the identification of instabilities with Neural Networks on JET", 2nd International conference Frontiers in diagnostic technologies, Frascati, 28-30 November 2011.

Acknowledgement

First, I would like to thank my parents for allowing me to realize my own potential. All the support they have provided me was the greatest gift anyone has ever given me.
Also, I would express my deep gratitude to my coordinator Prof. Luigi Fortuna for his invaluable guidance that began long before this PhD course. Without his precious mentorship it would not have been possible to complete this PhD thesis.
I would like to show special thanks to Prof. Mattia Frasca for his constructive feedbacks, comments, and for all the time invested in the supervision of my activities and thesis.
I also want to thank Eng. Arturo Buscarino who gave me technical support for all the projects we have been involved with together.
My gratitude is also extended to Prof. Salvatore Graziani, Prof. Giuliano Cammarata and Eng. Giuseppe Petrone with whom I had the pleasure to share an intriguing project on power electronic modules. It was a challenging experience being part of a multidisciplinary team of high qualified Professors and research Engineers.
I owe many thanks to Eng. Gianni Vitale and Eng. Natale Testa from STMicroelectronics for their precious support during the project on thermal characterization of high voltage power modules, It was a great pleasure working with them.
I must express my sincere gratitude to Prof. Francesco Iachello who allowed me to join the Department of Physics during my visiting period at Yale. He is one of the greatest person I have ever met in my life so far.
It gives me immense pleasure to thank Prof. Kumpati S. Narendra who welcomed me in his research team at the School of Engineering during my experience at Yale. The opportunity to work with him and his research team was one of the best professional experience so far. My thanks also goes to my former teammates and friends Eng. Prashanth Harshangi and Eng. Yu Wang for their support and encouragement during my period at Yale.
Last but not least, I thank my fellow labmates and friends Viviana, Nino, Davide and Carlo for all the stimulating discussions and for all the fun we have had in the last three years.